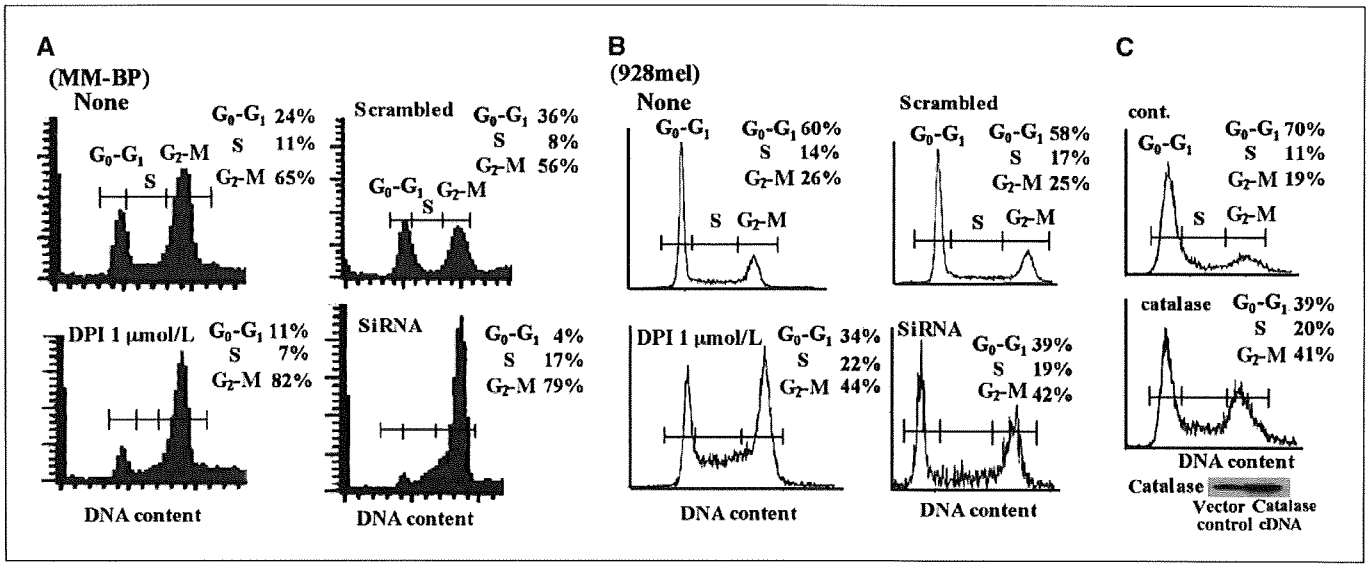

Figure 3. Cell-cycle perturbation by DPI, siNox4 RNAs, and catalase. *A,* parental MM-BP cells were serum-starved for 48 h and treated with or without 2 μmol/L DPI for 24 h (*left*). Alternatively, the cell lines carrying Nox4siRNAs or scrambled siRNAs were serum-starved for 48 h (*right*). Cells were then refed with the growth medium for 72 h and subjected to flow cytometric analysis. The proportion of nuclei in each pair of the cell cycle is shown. Similar results were obtained in three separate experiments. *B,* 928mel cells were serum starved, treated with or without DPI as in *A* (*left*). Alternatively, 928mel cells were transiently transfected with Nox4siRNAs or scrambled siRNAs and serum starved (*right*). Cells were then refed with the growth medium for 72 h and subjected to flow cytometric analysis. Similar results were obtained in three separate experiments. *C,* transfection of catalase increases G_2-M cell cycle arrest. MM-BP cells (10^5) were transfected with 5 μg of control vectors or pS-CAT (*catalase*), serum-starved for 48 h, and refed with the growth medium for 48 h. Cells were then analyzed for DNA content by flow cytometry. Similar results were obtained in three separate experiments. Expression of transfected catalase was determined by immunoblotting (*IB*) with anticatalase antibodies. *IP,* immunoprecipitation.

that Nox4siRNAs caused a significant reduction in anchorage-independent growth of MM-BP cells compared with that caused by scrambled siRNAs (Fig. 2*C*). The inhibitory effect of Nox4siRNAs on cell growth was detected in liquid culture, as well (Fig. 2*C*). These data indicate that Nox4-generated ROS are required to sustain growth of melanoma cells.

Suppression of tumor formation by Nox4siRNAs. Inhibition of anchorage-independent growth of MM-BP cells by Nox4siRNAs (Fig. 2*C*) suggests that silencing of Nox4 by Nox4siRNAs suppresses transformation phenotype of the cells. To test whether MM-BP cells become less tumorigenic through overexpression of Nox4siRNAs, the cells transfected with either scrambled or Nox4siRNAs were implanted into athymic nude mice. Although scrambled siRNA-transfected cells formed significant tumors in 2 weeks, introduction of Nox4siRNAs markedly decreased tumor growth (Fig. 2*D*). Thus, the results indicate that Nox4siRNAs inhibit tumorigencity of MM-BP cells, suggesting the critical mediating role of Nox4-derived ROS in development of some types of melanomas.

Because tumor progression is often associated with augmented cell motility and invasiveness of cancer cells, we compared scrambled siRNA-transfected cells with Nox4siRNA-transfected cells for the cell migration activity by Matrigel assay, but the migration was not suppressed by inhibition of Nox4 (Supplementary Fig. S3), implying that Nox4 is not involved in the regulation of the motility of MM-BP cells.

Inhibition of Nox4 induces cell cycle arrest. To further analyze the mechanism underlying Nox4siRNA-induced growth inhibition, cell cycle distribution of MM-BP cells was analyzed by flow cytometry. Cells were serum starved for 48 h to arrest their growth and refed with the growth medium in the presence or absence of DPI. Of note, treatment of MM-BP cells with DPI for 24 hours was found to induce an accumulation of cells in G_2-M phase (Fig. 3*A*). A marked increase of cell population in G_2-M phase was also observed with the cell line, siRNA1-a (Fig. 3*A*). Similarly, another Nox4-positive melanoma cell line, 928mel (Table 1) displayed cell accumulation in G_2-M phase when treated with DPI or transiently transfected with Nox4siRNAs (Fig. 3*B*). Furthermore, depletion of hydrogen peroxide by overexpression of catalase in MM-BP cells resulted in G_2-M cell cycle arrest (Fig. 3*C*), which is consistent with the notion that Nox4-derived ROS mediate cell cycle progression from G_2-M phase.

To characterize the molecular machinery involved in G_2-M cell cycle arrest upon ablation of Nox4, the expression of some of cell cycle–controlling genes was examined. A protein kinase CDK1 (cdc2) plays an important role in the regulation of the G_2-M cell cycle phase. Activation of CDK1 (dephosphorylation at Tyr-15) is required for transition from the G_2-M phase, whereas its inactivation (phosphorylation at Tyr-15) causes G_2-M cell cycle block (20). We therefore examined the phosphorylation state of the Tyr-15 of CDK1 by immunoblotting with anti-phospho CDK1 (Tyr-15) antibodies. The level of Tyr-15 phosphorylation was increased in MM-BP cells 24 hours after exposure to DPI (Fig. 4*A*), which chronologically coincided with induction of G_2-M phase cell cycle arrest by DPI treatment. Moreover, introduction of Nox4siRNAs into MM-BP cells resulted in a similar increase in Tyr-15 phosphorylation of CDK1 compared with that in scrambled siRNA-transfected cells (Fig. 4*A*). The total amount of CDK1 proteins was not changed (data not shown). Likewise, Tyr-15 phosphorylation of CDK1 was induced in DPI-treated or Nox4siRNA-transfected melanoma 928mel cells (Fig. 4*A*). These data suggest that the G_2-M cell cycle arrest was induced as CDK1 was inactivated. p53 and $p21^{WAF1/CIP1}$, such as CDK1, have been reported to regulate the G_2-M transition and be critical in sustaining the G_2-M cell cycle arrest after DNA damage through inhibition of CDK1 (21, 22). DPI treatment had no

appreciable effect on either p53 or $p21^{WAF1/CIP1}$ protein levels in MM-BP cells for at least 24 hours, as determined by immunoblotting analysis (Fig. 4*B*). These results suggest that induction of G_2-M arrest by Nox4 inhibition is controlled by a mechanism independent of both p53 and $p21^{WAF1/CIP1}$.

It has been known that the activity of CDK1 is regulated by cdc25c phosphatase through dephosphorylation of the Tyr-15 residue, and that the activity of cdc25c is modulated by phosphorylation. To determine whether phosphorylation of cdc25c was regulated by Nox4, we analyzed fractions of cdc25c mobility by immunoblotting. Consistent with the previous report (23), the unphosphorylated form "a" and phosphorylated form "b" (Ser216 phosphorylation) of cdc25c were detected in untreated MM-BP cells (Fig. 4*C*). In contrast, addition of DPI for 24 hours induced hyperphosphorylation of cdc25c, which is indicated by the appearance of a slower-migrated form "c" of cdc25c (refs. 23, 24; Fig. 4*C*). Similarly, the level of the hyperphosphorylated cdc25c protein was elevated in a Nox4siRNA-transfected MM-BP cell line, whereas it was not increased in scrambled siRNA-transfected cells (Fig. 4*C*). Hyperphosphorylation of cdc25c is thought to prolong its remaining in the cytoplasm due to increased binding with 14-3-3 proteins, inhibiting the interaction between cdc25c and CDK1 in the nucleus (19, 25). Indeed, immunostaining showed that exclusion of cdc25c from the nuclei was increased in both DPI-exposed and Nox4siRNA-transfected MM-BP cells (Fig. 4*D*). Coprecipitation studies showed that Nox4siRNA transfection resulted in enhanced binding of cdc25c with 14-3-3 when compared with scrambled siRNAs transfection (Fig. 4*D*). Thus, these data suggest that hyperphosphorylation of cdc25c mediates both DPI and Nox4siRNA-induced Tyr-15 phosphorylation of CDK1, leading to cell cycle arrest at G_2-M stage.

The growth inhibition is frequently accompanied by induction of apoptosis. By using terminal deoxynucleotidyl-transferase–mediated dUTP nick-end labeling assay, we therefore examined whether or not suppression of the Nox4 activity induces apoptosis. No significant changes in cell survival rate were detected after DPI or Nox4siRNA treatment (Supplementary Fig. S4), which is consistent with the flow cytometric profiles without any sub-G_1 peak representing apoptotic cell population (Fig. 3*A* and *B*). From these data, we conclude that the observed growth inhibitory effects of DPI and Nox4siRNAs in both soft agar and liquid culture are due to cell cycle arrest at G_2-M transition rather than apoptosis.

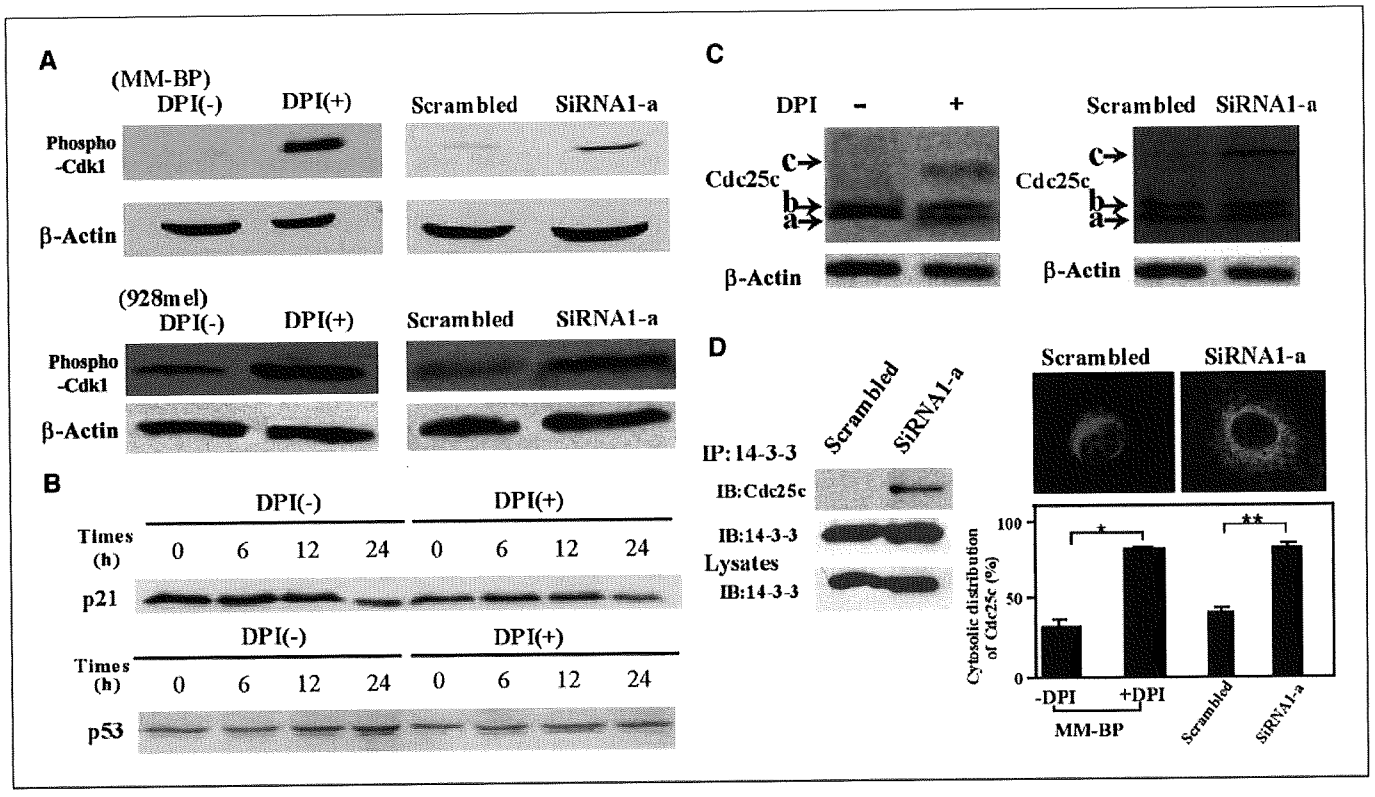

Figure 4. Effects of DPI and Nox4 siRNAs on G_2-M phase cell cycle controlling proteins. *A*, MM-BP cells were serum-starved, treated with or without DPI (2 μmol/L), and refed in growth media as in Fig. 3*A*. Alternatively, the cell line siRNA1-a or scrambled was serum-starved and refed in growth media as above. Then, cell lysates were subjected to immunoblotting with anti-phospho CDK1 (tyr-15) antibodies (*top*). 928mel cells were serum starved for 48 h, treated with or without DPI (2 μmol/L) for 24 h, and refed in growth media for 72 h. Alternatively, 928mel cells transiently transfected with Nox4siRNAs or scrambled siRNAs were serum starved and refed with growth media as above. Lysates were subjected to immunoblotting using anti-phospho (Tyr-15) CDK1 antibodies (*bottom*). *B*, MM-BP cells were incubated with or without DPI (2 μmol/L) for the indicated time periods. Cell lysates were processed for immunoblotting using antibodies to $p21^{WAF1/CIP1}$ or p53. *C*, DPI or Nox4siRNA-induced hyperphosphorylation of cdc25c. MM-BP cells were serum starved for 48 h and treated with 2 μmol/L DPI for 15 h. Alternatively, cell lines, siRNA1-a or scrambled were serum starved for 48 h and refed with the growth medium. Lysates were subjected to immunoblotting with anti-cdc25c antibodies. Note that form a and b bands partially overlapped due to overloading samples. Protein loading was monitored by β-actin. *D*, MM-BP cells were treated with or without DPI as in *A*. Cell lines, scrambled and siRNA1-a were serum starved and refed with complete growth medium for 24 h as in *A*. Cells were fixed and stained with rabbit anti-cdc25c antibodies and CY-3–conjugated anti-rabbit IgG antibodies (Molecular Probes). *Right*, immunostained patterns. Histograms show means ± SD of 3 separate experiment (average number of counted cells is 80). $P < 0.05$ (*) and $P < 0.05$ (**) versus DPI (−) and scrambled, respectively. After serum starvation/refeeding, lysates prepared from scrambled or siRNA 1-a cells were immunoprecipitated with anti–14-3-3 antibodies, followed by immunoblotting with anti-cdc25c antibodies (*left*). 14-3-3 proteins in lysates and immunoprecipitates were identified by immunoblotting with 14-3-3 antibodies.

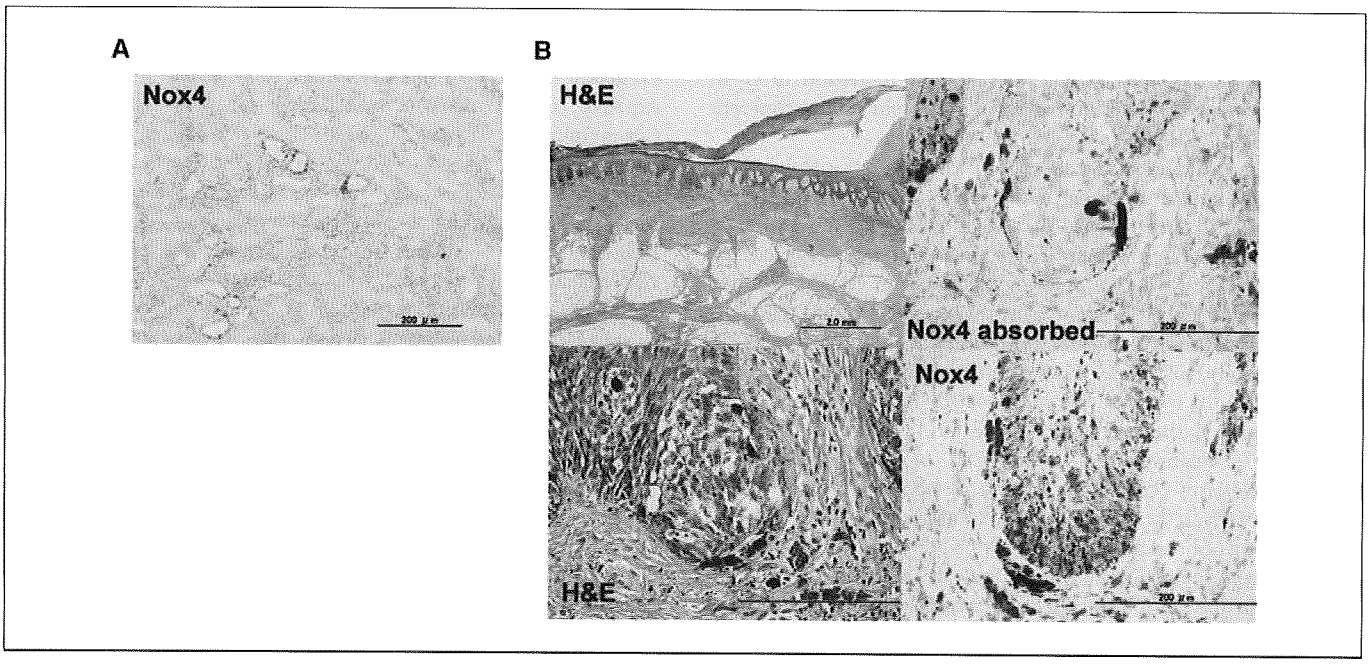

Figure 5. Expression of Nox4 in melanoma tissues. Biopsy specimens of melanoma were surgically isolated and immunohistochemistry with rabbit anti-Nox4 antibodies were performed. Nox4-positive melanoma cells were found in the epidermal nest (*B, Nox4*). Immunoadsorption of the antibodies with the Nox4 peptide antigen abolished Nox4 staining (*B, Nox4 adsorbed*). In control experiments (*A*), the antibodies detected Nox4 expression in normal renal cortex as reported (26). Tissues were counterstained with hematoxylin.

Expression of Nox4 in melanoma tissues. To examine whether Nox4 expression is really up-regulated in melanoma tissues, Nox4 expression patterns were evaluated in 13 primary or metastatic melanoma samples isolated from patients by immunohistochemistry using antibodies against Nox4. Immunoblotting analysis showed that the raised Nox4 antibodies recognize Nox4 proteins (Supplementary Fig. S2). The result was then confirmed by showing the staining of the proximal renal tubles of normal kidney with the antibodies as reported earlier (Fig. 5*A*; ref. 26). Nox4 was expressed in 4 of 13 melanoma tissues, including 5 acral melanomas, 6 superficial spending melanomas, 1 nodular melanoma, and 1 mucosal melanoma (Table 1). Of these, two acral melanomas and two superficial spending melanomas expressed Nox4. Frequency of Nox4 expression seemed independent of clinical type. Interestingly, Nox4 was strongly expressed in the nests in epidermis (Fig. 5*B*) but less in the metastatic lymph nodes. In all of the Nox4-positive melanoma tissues, Nox4 was localized in the cytoplasm or perinucleus. Immunoabsorption of the antibodies with the Nox4 peptide antigen abolished most of the staining, indicating that the staining is Nox4 specific (Fig. 5*B*). No Nox4 expression was observed in normal skin tissues and cultured melanocytes (data not shown). These observations show that Nox4 is expressed not only in cultured melanoma cell lines but indeed in melanoma tissues, which lends additional support to the view that Nox4 plays some important role in pathogenesis of melanoma.

Discussion

Malignant melanoma is the most aggressive form of skin cancer. ROS production has been partly implicated in the development of melanoma and its resistance to radiation and chemotherapy, but the functional roles of ROS are not fully understood. Here, we show that superoxide generation by Nox4 is required for proliferation of melanoma MM-BP cells and formation of tumors derived from MM-BP cells in athymic mice, suggesting a critical role for Nox4 in maintenance of malignant transformation phenotype of melanoma. Furthermore, our studies reveal that Nox4 mediates cell proliferation by regulating G_2-M cell cycle progression because inhibition of Nox4 activity by either Nox4-specific siRNAs or DPI caused G_2-M cell cycle arrest. This is also supported by the facts that G_2-M arrest upon Nox4 inhibition was observed in another melanoma cell line, 928mel, and that G_2-M block was induced by catalase-mediated depletion of hydrogen peroxide, a dismutated metabolite of Nox4-generated superoxide. To our knowledge, this is the first observation that Nox enzyme–mediated signalings link to the cell cycle controlling events.

CDK1 (cdc2) kinase that interacts with cyclin B is a key mitosis-promoting kinase in the control of the G_2-M cell cycle progression. Namely, activation of CDK1, complexed with cyclin B, promotes transition from G_2 to M phase of the cell cycle. CDK1 is activated by cdc25c phosphatase that dephosphorylates CDK1 at Tyr-15 residues. Our data indicate that both Nox4siRNAs and DPI treatment inactivate cdc25c, causing increased phosphorylation of CDK1 on Tyr-15, a hallmark of the G_2-M checkpoint. The activity of cdc25c is believed to be inactivated mainly by two mechanisms: (*a*) phosphorylation of cdc25c at Thr-47 decreases its phosphatase activity; (*b*) hyperphosphorylation of cdc25c creates a binding site for 14-3-3 proteins, which sequester cdc25c to the cytoplasm and thereby interfere with its interaction with CDK1 in the nucleus (19, 25). As abrogation of Nox4-generated ROS led to induction of hyperphosphorylated cdc25c, the most-likely possibility is that the G_2-M cell cycle arrest was caused via the second mechanism. Although p53 and $p21^{WAF1/C2P1}$ have also been implicated in regulation of the G_2-M cell cycle arrest after DNA damage through inhibition of CDK1 (21, 22), the expression levels of p53 and $p21^{WAF1/C2P1}$ were unaffected by suppression of the Nox4 activity

(Fig. 4*B*), rendering their involvement unlikely. The elevated expression of cyclin D and CDK4, critical gatekeepers at the G_1-S check point and targets to the Ras-B-Raf pathway, is frequently found in melanoma (27, 28). The dysfunction of these cell cycle controlling genes is considered to result in abnormal proliferation of melanoma cells (29). Thus, our observation would be significant in the sense that it revealed an alternative deregulation of melanoma cell growth depending on the aberrant control of a G_2-M checkpoint. It will be of interest in future studies to identify a molecule(s) mediating a signal transmission from Nox4-generated ROS to cdc25c-CDK1 connection.

Immunohistochemical experiments revealed that Nox4 expression was increased in tissues obtained from several types of melanoma biopsies, whereas no expression of Nox4 was detected in normal tissues adjacent to the tumor. Evidence indicates that expression of Nox4 is augmented not only in human melanoma cell lines but indeed occurs during *in vivo* melanoma development. Notably, melanoma in epidermis contains a high level of Nox4, but metastatic melanoma in lymph nodes exhibits a decrease in the Nox4 level. Elevated ROS production by up-regulated Nox enzymes may increase a risk of cancer in early stages by causing persistent proinflammatory responses (30). At least, Nox4 does not seem to contribute to the motile activity of melanoma cells, which is related to invasiveness of tumors (see Result).

Overall, our study showed the functional requirement of Nox4-generated ROS for transformation phenotype associated with melanoma and revealed a novel cell cycle regulation effect of Nox4 in melanoma cells. The discovery has significant implications in understanding the molecular mechanism of melanocyte tumor development and Nox4 could be a potential molecular target in the treatment of melanoma.

Disclosure of Potential Conflicts of Interest

No potential conflicts of interest were disclosed.

Acknowledgments

Received 10/1/2008; revised 12/1/2008; accepted 12/29/2008; published OnlineFirst 3/10/09.

Grant support: Grant on Cancer Research in Applied Areas from the Ministry of Science and Culture of Japan (T. Kamata).

The costs of publication of this article were defrayed in part by the payment of page charges. This article must therefore be hereby marked *advertisement* in accordance with 18 U.S.C. Section 1734 solely to indicate this fact.

We thank Dr. T. Finkel for catalase plasmid and technical assistance for M. Ito and PY. Zhang, Dr. N. Colburn for a critical reading of the manuscript and, F. Ushiyama for typing the manuscript.

References

1. Lambeth JD. NOX enzymes and the biology of reactive oxygen. Nat Rev Immunol 2004;4:181–9.
2. Lassegue B, Sorescu D, Szocs K, et al. Novel gp91(phox) homologues in vascular smooth muscle cells: nox1 mediates angiotensin II-induced superoxide formation and redox-sensitive signaling pathways. Circ Res 2001;88:888–94.
3. Suh YA, Arnold RS, Lassegue B, et al. Cell transformation by the superoxide-generating oxidase Mox1. Nature 1999;401:79–82.
4. Mitsushita J, Lambeth JD, Kamata T. The superoxide-generating oxidase Nox1 is functionally required for Ras oncogene transformation. Cancer Res 2004;64:3580–5.
5. Pedruzzi E, Guichard C, Ollivier V, et al. NAD(P)H oxidase Nox-4 mediates 7-ketocholesterol-induced endoplasmic reticulum stress and apoptosis in human aortic smooth muscle cells. Mol Cell Biol 2004;24:10703–17.
6. Park HS, Jung HY, Park EY, Kim J, Lee WJ, Bae YS. Cutting edge: direct interaction of TLR4 with NAD(P)H oxidase 4 isozyme is essential for lipopolysaccharide-induced production of reactive oxygen species and activation of NF-κB. J Immunol 2004;173:3589–93.
7. Szatrowski TP, Nathan CF. Production of large amounts of hydrogen peroxide by human tumor cells. Cancer Res 1991;51:794–8.
8. Shinohara M, Shang WH, Kubodera M, et al. Nox1 redox signaling mediates oncogenic Ras-induced disruption of stress fibers and focal adhesions by down-regulating Rho. J Biol Chem 2007;282:17640–8.
9. Vaquero EC, Edderkaoui M, Pandol SJ, Gukovsky I, Gukovskaya AS. Reactive oxygen species produced by NAD(P)H oxidase inhibit apoptosis in pancreatic cancer cells. J Biol Chem 2004;279:34643–54.
10. Mochizuki T, Furuta S, Mitsushita J, et al. Inhibition of NADPH oxidase 4 activates apoptosis via the AKT/apoptosis signal-regulating kinase 1 pathway in pancreatic cancer PANC-1 cells. Oncogene 2006;25:3699–707.
11. Brar SS, Corbin Z, Kennedy TP, et al. NOX5 NAD(P)H oxidase regulates growth and apoptosis in DU 145 prostate cancer cells. Am J Physiol Cell Physiol 2003;285: C353–69.
12. Fu X, Beer DG, Behar J, Wands J, Lambeth D, Cao W. cAMP-response element-binding protein mediates acid-induced NADPH oxidase NOX5-S expression in Barrett esophageal adenocarcinoma cells. J Biol Chem 2006;281: 20368–82.
13. Sander CS, Hamm F, Elsner P, Thiele JJ. Oxidative stress in malignant melanoma and non-melanoma skin cancer. Br J Dermatol 2003;148:913–22.
14. Church SL, Grant JW, Ridnour LA, et al. Increased manganese superoxide dismutase expression suppresses the malignant phenotype of human melanoma cells. Proc Natl Acad Sci U S A 1993;90:3113–7.
15. Prasad KN, Edwards-Prasad J. Effects of tocopherol (vitamin E) acid succinate on morphological alterations and growth inhibition in melanoma cells in culture. Cancer Res 1982;42:550–5.
16. Valencia A, Kochevar IE. Nox1-based NADPH oxidase is the major source of UVA-induced reactive oxygen species in human keratinocytes. J Invest Dermatol 2008; 128:214–22.
17. Brar SS, Kennedy TP, Sturrock AB, et al. An NAD(P)H oxidase regulates growth and transcription in melanoma cells. Am J Physiol Cell Physiol 2002;282:C1212–24.
18. Byers HR, Etoh T, Doherty JR, Sober AJ, Mihm MC, Jr. Cell migration and actin organization in cultured human primary, recurrent cutaneous and metastatic melanoma. Time-lapse and image analysis. Am J Pathol 1991;139:423–35.
19. Lee MS, Ogg S, Xu M, et al. cdc25+ encodes a protein phosphatase that dephosphorylates p34cdc2. Mol Biol Cell 1992;3:73–84.
20. Harper JW, Adami GR, Wei N, Keyomarsi K, Elledge SJ. The p21 Cdk-interacting protein Cip1 is a potent inhibitor of G1 cyclin-dependent kinases. Cell 1993;75: 805–16.
21. Xiong Y, Hannon GJ, Zhang H, Casso D, Kobayashi R, Beach D. p21 is a universal inhibitor of cyclin kinases. Nature 1993;366:701–4.
22. Peng CY, Graves PR, Thoma RS, Wu Z, Shaw AS, Piwnica-Worms H. Mitotic and G2 checkpoint control: regulation of 14–3-3 protein binding by phosphorylation of Cdc25C on serine-216. Science 1997;277:1501–5.
23. Herman-Antosiewicz A, Singh SV. Checkpoint kinase 1 regulates diallyl trisulfide-induced mitotic arrest in human prostate cancer cells. J Biol Chem 2005;280: 28519–28.
24. Kumagai A, Dunphy WG. Binding of 14–3-3 proteins and nuclear export control the intracellular localization of the mitotic inducer Cdc25. Genes Dev 1999;13: 1067–72.
25. Xiao D, Herman-Antosiewicz A, Antosiewicz J, et al. Diallyltrisulfide-induced G(2)-M phase cell cycle arrest in human prostate cancer cells is caused by reactive oxygen species-dependent destruction and hyperphosphorylation of Cdc 25 C. Oncogene 2005;24:6256–68.
26. Geiszt M, Kopp JB, Varnai P, Leto TL. Identification of renox, an NAD(P)H oxidase in kidney. Proc Natl Acad Sci U S A 2000;97:8010–4.
27. Serrano M, Lee H, Chin L, Cordon-Cardo C, Beach D, DePinho RA. Role of the INK4a locus in tumor suppression and cell mortality. Cell 1996;85:27–37.
28. Curtin JA, Fridlyand J, Kageshita T, et al. Distinct sets of genetic alterations in melanoma. N Engl J Med 2005; 353:2135–47.
29. Takata M, Saida T. Genetic alterations in melanocytic tumors. J Dermatol Sci 2006;43:1–10.
30. Murakami S, Noguchi T, Takeda K, Ichijo H. Stress signaling in cancer. Cancer Sci 2007;98:1521–7.

	JNCI	djp309	JY
	JOURNAL NAME	Art. No.	CE Code

BRIEF COMMUNICATION

Polyclonality of *BRAF* Mutations in Acquired Melanocytic Nevi

Jingrong Lin, Minoru Takata, Hiroshi Murata, Yasufumi Goto, Kenji Kido, Soldano Ferrone, Toshiaki Saida

Melanocytic nevi are thought to be senescent clones of melanocytes that have acquired an oncogenic *BRAF* mutation. *BRAF* mutation is considered to be a crucial step in the initiation of melanocyte transformation. However, using immunomagnetic separation or laser-capture microdissection, we examined *BRAF* mutations in sets of approximately 50 single cells isolated from acquired melanocytic nevi from 13 patients and found a substantial number of nevus cells that contained wild-type *BRAF* mixed with nevus cells that contained $BRAF^{V600E}$. Furthermore, we simultaneously amplified *BRAF* exon 15 and a neighboring single nucleotide polymorphism (SNP), rs7801086, from nevus cell samples obtained from four patients who were heterozygous for this SNP. Subcloning and sequencing of the polymerase chain reaction products showed that both SNP alleles harbored the $BRAF^{V600E}$ mutation, indicating that the same $BRAF^{V600E}$ mutation originated from different cells. The polyclonality of *BRAF* mutations in acquired melanocytic nevi suggests that mutation of *BRAF* may not be an initial event in melanocyte transformation.

J Natl Cancer Inst 2009;101:1–5

v-raf murine sarcoma viral oncogene homolog B1 (*BRAF*) is a member of the *raf* gene family that encodes a cytoplasmic serine/threonine kinase that signals in the mitogen-activated protein kinase pathway and mediates cell proliferation and differentiation. Mutations in the *BRAF* gene, most commonly including $BRAF^{V600E}$, which encodes an amino acid substitution that leads to RAS-independent autoactivation of the BRAF kinase with subsequent stimulation of the downstream kinases and transcription factors, have been frequently found in melanoma lesions and melanocytic nevi (1,2). This finding has been interpreted to suggest that mutation of *BRAF* is a crucial step in the initiation of melanocyte transformation (2). Furthermore, two recent studies have shown that sustained $BRAF^{V600E}$ expression in normal melanocytes causes either cell cycle arrest accompanied by the induction of both $p16^{INK4a}$ protein expression and senescence-associated acidic β-galactosidase activity (3) or substantial reduction of cell proliferation accompanied by the induction of nuclear $p16^{INK4a}$ expression (4). Both $p16^{INK4a}$ protein expression and acidic β-galactosidase activity were also demonstrated in melanocytic nevi in situ (3,4). These results suggest that melanocytic nevi are benign tumors that originate from the clonal expansion of a single melanocyte that acquires a $BRAF^{V600E}$ mutation and temporarily proliferates in response to oncogenic *BRAF* signaling, followed by growth arrest due to oncogene-induced senescence (5).

However, in a recent analysis of *BRAF* mutations in a large series of melanocytic nevi (6), we observed clonal heterogeneity in terms of *BRAF* mutations among the cells in a few small congenital nevi (6). Because of these findings and the possibility that they contradict the currently accepted model of melanocytic neoplastic progression (5), we tested the polyclonality of *BRAF* mutations in acquired melanocytic nevi.

The study was approved by the medical ethics committee of the Shinshu University School of Medicine. All patients gave written informed consent. We obtained acquired melanocytic nevi from 14 patients. After bisection, one-half of the nevus tissue was routinely fixed and embedded in paraffin. The other half was used to isolate single nevus cells. For six nevi (numbers 1–6 in Table 1), we removed the epidermis, minced the tissue, and collected nevus cells using a cocktail of human high molecular weight-melanoma-associated antigen (HMW-MAA)–specific monoclonal antibodies and magnetic beads (Dynabeads CELLection Pan Mouse IgG Kit; Invitrogen Dynal AS, Oslo, Norway), as described previously (7). Separated nevus cells were smeared on film-coated glass slides (Meiwafosis Co Ltd, Osaka, Japan) and subjected to laser-capture microdissection using a PALM-MB microdissection system (PALM Microlaser technologies, Bernried, Germany) to isolate approximately 60–65 cells.

Immunohistochemical staining with monoclonal antibodies showed high levels of expression of HMW-MAA on nevus cells (Supplementary Figure 1, available online). No staining of melanocytes was detected. Although a few keratinocytes within the hair follicles and the basal layer of the epidermis expressed HMW-MAA, as reported previously (8), virtually no cells were captured when we performed immunomagnetic cell separation using normal skin. To further confirm the specificity of the nevus cell isolation, we stained the immunomagnetically separated cells with a rabbit polyclonal anti–S-100 antibody (Dako, Glostrup, Denmark) (1:300 dilution) followed by DAKO Envision System (Dako, Carpinteria, CA), for three samples (sample numbers 3–5), and observed positive staining for almost all of the separated cells.

For the remaining eight nevi (numbers 7–14 in Table 1), one-half of the nevus tissue was snap frozen in optimal cutting temperature compound, cut 6 μm thick, stained with toluidine blue, and subjected to laser-capture microdissection. Approximately 60–65 isolated single nevus cells were collected into lysis buffer containing 10 mM Tris–HCl (pH 8.3), 50 mM KCl, 4 mg/mL proteinase

Affiliations of authors: Department of Dermatology, Shinshu University School of Medicine, Matsumoto, Japan (JL, MT, HM, YG, KK, TS); Department of Surgery, Department of Immunology, and Department of Pathology, University of Pittsburgh Cancer Institute, Pittsburgh, PA (SF).

Correspondence to: Minoru Takata, MD, Department of Dermatology, Shinshu University School of Medicine, Asahi 3-1-1, Matsumoto 390-8621, Japan (e-mail:mtakata@shinshu-u.ac.jp).

See "Funding" and "Notes" following "References."

DOI: 10.1093/jnci/djp309

CONTEXT AND CAVEATS

Prior knowledge

Oncogenic *BRAF* mutation has been considered to be an early step in the formation of melanocytic nevi, but recently, clonal heterogeneity was found in a few nevi.

Study design

Approximately 50 single cells were separated from each of 13 melanocytic nevi either by using immunomagnetic beads or by laser-capture microdissection and were subjected to single-cell polymerase chain reaction and sequencing to determine *BRAF* mutations. In another experiment, *BRAF* and a neighboring single-nucleotide polymorphism were simultaneously amplified from nevi of four patients who were heterozygous for the polymorphism.

Contribution

Although *BRAF* mutations were always found among nevus cells, cells that contained only wild-type *BRAF* predominated in nine of 13 nevi. When *BRAF* was sequenced from both alleles of four patients heterozygous for an adjacent polymorphism, both alleles harbored *BRAF* mutations.

Implications

These results suggest that *BRAF* may be mutated as a late event in melanocytic tumorigenesis.

Limitations

A small number of nevi of only two histological types were examined.

From the Editors

K (Roche Diagnostics, Basel, Switzerland), and 3% Tween 20 and incubated for 16 hours at 50°C (6). We amplified exon 15 of the gene using heminested polymerase chain reaction (PCR) (Supplementary Table 1, available online). PCR products were purified and sequenced using the BigDye Terminator v3.1 cycle sequencing kit (Applied Biosystems, Foster City, CA). To prevent potential contamination, aerosol resistant tips with filters were used and gloves and a mask were worn at all times. Samples without target DNA and/or DNA from single epidermal keratinocytes containing wild-type *BRAF* (similarly isolated by laser-capture microdissection) were always included as negative controls to monitor PCR contamination.

We successfully isolated single nevus cells from immunomagnetically captured cell smears and from frozen tissue sections (Figure 1, A and B). The success rate of PCR amplification from single cells ranged from 74% to 85%, and we obtained *BRAF* sequences from approximately 50 single nevus cells for each patient sample. Sequence analyses revealed that all the 13 samples of the acquired melanocytic nevi contained nevus cells that had wild-type *BRAF* and cells that were heterozygous for $BRAF^{V600E}$ (Table 1). Nevus cells containing wild-type *BRAF* predominated in nine of 13 nevi. Consistent with the results of our previous study (6), nevus cells harboring *BRAF* mutations were very rarely detected in the two acral nevi that we examined (sample numbers 12 and 13) compared with nevi from other sites, which suggested a possible role for UV exposure in the acquisition of *BRAF* mutations in acquired melanocytic nevi. Cells with rare *BRAF* mutations, such as $BRAF^{V600K}$, $BRAF^{V600A}$, $BRAF^{V600E/G}$, and $BRAF^{T599I}$, all of which have been previously described in melanoma lesions (http://www.sanger.ac.uk/genetics/CGP/cosmic), were found in three nevi (numbers 4, 7, and 9). Except for one compound heterozygous mutation of $BRAF^{V600E/G}$ that was identified in sample number 9 (Figure 1, B), all of the other variant mutations were heterozygous. The protein products of two of these variant mutations ($BRAF^{T599I}$ and $BRAF^{V600K}$) were shown to have much lower kinase activity compared with $BRAF^{V600E}$ (9). Thus, cell clones harboring these variant mutations may have weaker growth advantage than those with the $BRAF^{V600E}$ mutation, and may have been overlooked in the previous conventional sequence analyses, because the heterozygous mutation could be reliably discernible only when the samples contained more than 20% of clonal mutant cells (6).

Detection of the homozygous $BRAF^{V600E}$ mutation in a few single cells was considered to be due to the failure of PCR to amplify the wild-type allele, that is, allele dropout, which is a common problem in single-cell PCR (10). To assess the actual frequency of allele dropout, we performed a control experiment using the melanoma cell line 928mel, which is known to harbor the heterozygous $BRAF^{V600E}$ mutation (11). Using the methodology used to obtain single nevus cells, single melanoma cells were isolated by laser-capture microdissection either from immunomagnetically captured cell smears or 6-μm cryosections of cells suspended in agarose and embedded in optimal cutting temperature compound. We found wild-type *BRAF* sequences and homozygous $BRAF^{V600E}$ mutations, both of which were thought to be due to allele dropout, in three of 50 (6%) single melanoma cells isolated by immunomagnetic beads and in 12 of 50 (24%) of those obtained from 6-μm frozen sections. The much higher frequency of allele dropout in the latter is explained by the nuclear damage during tissue sectioning. This was reflected in the results that showed a lower frequency of homozygous $BRAF^{V600E}$ mutations in samples obtained by immunomagnetic isolation (numbers 1–6) than frozen tissue sections (numbers 8–13). Then, we conducted a two-sided binomial test for each nevus sample using the 95% confidence limits of allele dropout in control melanoma cells as the test proportion, that is, 0.11 for immunomagnetic cell separation and 0.27 for frozen tissue sections. We used SPSS 15.0 software package (SPSS Inc, Tokyo, Japan) for this analysis. At the statistical significance level of .05, the possibility that all of the wild-type sequences were due to drop out of the mutant alleles was denied in all but one nevus (number 11), indicating that most acquired melanocytic nevi were composed of both *BRAF*-mutated cells and *BRAF*-wild-type cells.

We then further investigated whether *BRAF* mutant cells in acquired melanocytic nevi are monoclonal or polyclonal. For this purpose, we examined four acquired melanocytic nevi (numbers 3, 6, 11, and 14) that were excised from patients who were heterozygous for the single nucleotide polymorphism (SNP) rs7801086 (GCCG AGA vs GCCTAGA) (Figure 1, C). This SNP maps to chromosome 7, about 2 kb telomeric from exon 15 of the *BRAF* gene. We obtained pure nevus cell populations (but not single nevus cells) from bisected nevus tissues either by using immunomagnetic beads with HMW-MAA–specific monoclonal antibodies (for sample numbers 3 and 6) or by laser-capture microdissection of multiple nevus cell nests from 6-μm frozen tissue sections (for sample numbers 11 and 14). After simultaneous amplification of DNA fragments containing both *BRAF*

Table 1. Polyclonality of *BRAF* mutations in acquired melanocytic nevi as revealed by single-cell polymerase chain reaction (PCR) and sequencing of DNA from approximately 50 cells per nevus*

Sample No.	Age, y	Sex	Site	Histology (Type)	Method	No. of cells with wild-type *BRAF*	No. of cells with heterozygous V600E mutation	No. of cells with other *BRAF* mutations†	No. of cells with homozygous V600E mutation	PCR failure	Total No. of cells (valid PCR)	*P*‡
N-1	34	F	Nose	Intradermal nevus (Miescher)	IMS	15	34	0	1	9	59 (50)	<.001
N-2	28	F	Abdomen	Intradermal nevus (Unna)	IMS	11	38	0	1	9	59 (50)	.018
N-3	31	F	Nose	Intradermal nevus (Miescher)	IMS	26	22	0	2	12	62 (50)	<.001
N-4	44	M	Face	Intradermal nevus (Miescher)	IMS	33	11	2 (V600K) 3 (T599I)	1	14	64 (50)	<.001
N-5	52	F	Neck	Intradermal nevus (Unna)	IMS	28	21	0	1	13	63 (50)	<.001
N-6	35	F	Face	Intradermal nevus (Miescher)	IMS	30	20	0	2	10	62 (52)	<.001
N-7	13	F	Abdomen	Intradermal nevus (Unna)	FTS	29	16	1 (V600A)	2	15	63 (48)	<.001
N-8	65	F	Nose	Compound nevus (Miescher)	FTS	31	14	0	5	9	59 (50)	<.001
N-9	81	M	Face	Compound nevus (Miescher)	FTS	21	23	1 (V600E/G)	4	16	65 (49)	.012
N-10	28	F	Arm	Intradermal nevus (Unna)	FTS	31	16	0	3	15	65 (50)	<.001
N-11	27	F	Face	Intradermal nevus (Miescher)	FTS	13	30	0	7	13	63 (50)	.510
N-12	25	F	Sole	Junctional nevus (Acral)	FTS	42	3	0	1	16	62 (46)	<.001
N-13	37	M	Sole	Compound nevus (Acral)	FTS	45	5	0	0	13	63 (50)	<.001
N-14	27	F	Abdomen	Intradermal nevus (Unna)	FTS	—	—	—	—	—	—	—
928mel	—	—	—	Melanoma cell line	IMS	1	47	0	2	13	63 (50)	—
928mel	—	—	—	Melanoma cell line	FTS	7	38	0	5	12	62 (50)	—

* FTS = Frozen tissue section. Six-μm cryosections were prepared from the nevus tissues or melanoma cell suspension embedded in agarose; IMS = Immunomagnetic cell separation using antibodies against human high molecular weight-melanoma-associated antigen.

† V600K, GT1798-99→AA; T599I, C1796→T; V600A, T1799→C; V600E/G, T1799→A + T1799→G.

‡ Two-sided binomial tests were conducted using the 95% confidence limit of each method (0.11 for IMS and 0.27 for FTS) with the null hypothesis that all the wild types were due to allele dropout.

exon 15 and SNP rs7801086 using the long-range Expand High Fidelity^{PLUS} PCR System (Roche Applied Science, Mannheim, Germany), we subcloned the PCR products of separate alleles in bacteria. We then sequenced *BRAF* exon 15 and SNP rs7801086 from 16 to 30 individual bacterial colonies (for PCR primers, see Supplementary Table 1, available online). Among the clones containing PCR products from each of the four acquired melanocytic nevi, we found both colonies that harbored the $BRAF^{V600E}$ (T1799→A) mutation and the T allele of SNP rs7801086 and colonies that harbored the $BRAF^{V600E}$

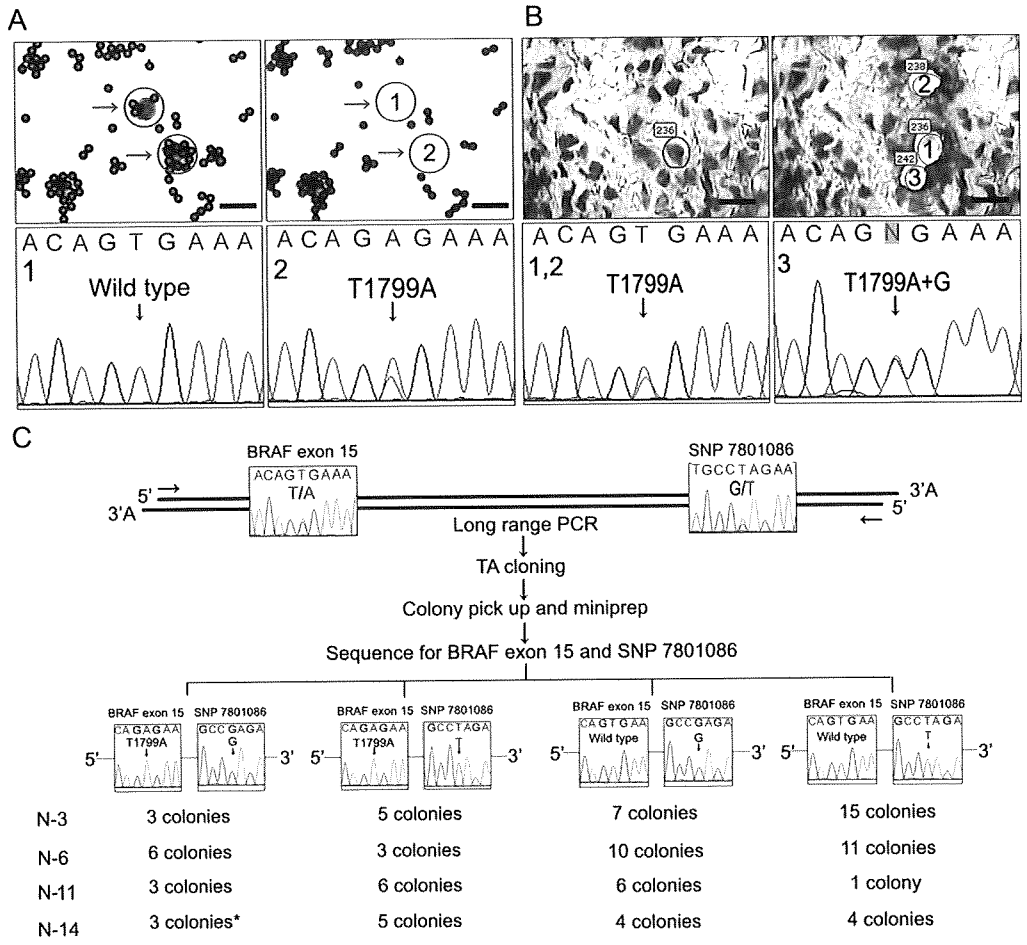

Figure 1. Polyclonality of *v-raf* murine sarcoma viral oncogene homolog B1 (*BRAF*) mutations in acquired melanocytic nevi. **A)** Selection of single nevus cells after immunomagnetic separation. Single nevus cells (**purple dots with arrows**) were captured by high molecular weight-melanoma-associated antigen–specific monoclonal antibodies bound to immunomagnetic beads (**pink dots**). The cells (**encircled**) were procured by laser-capture microdissection (**top**; bar = 20 μm). Polymerase chain reaction (PCR) amplification and subsequent sequencing of single nevus cells showed wild-type *BRAF* and $BRAF^{V600E}$ mutations (**bottom**). **B)** Laser-capture microdissection of frozen tissue section of acquired melanocytic nevi followed by direct sequencing of *BRAF* exon 15 (**top**; bar = 20 μm). Sequencing revealed two of the contiguous single nevus cells to have the $BRAF^{V600E}$ mutation and one to have a compound heterozygous $BRAF^{V600E}$ (T1799A) and $BRAF^{V600G}$ (T1799G) mutation, showing a heterogeneous pattern of *BRAF* mutations in proximal cells on a single-cell level (**bottom**). **C)** Subcloning and subsequent sequencing of *BRAF* exon 15 and the single nucleotide polymorphism (SNP) rs7801086. This SNP maps approximately 2 kb telomeric from *BRAF* exon 15. Four nevi (numbers 3, 6, 11, and 14) were excised from patients who were heterozygous for this SNP. DNA was extracted from hundreds of nevus cells isolated either by using immunomagnetic beads (numbers 3 and 6) or laser-capture microdissection of frozen tissue sections (numbers 11 and 14). A 2859-bp fragment containing both *BRAF* exon 15 and the SNP rs7801086 was amplified by long-range PCR. Subcloning was carried out using this fragment as an insert. Sixteen to 30 colonies were randomly picked from each patient sample and analyzed for the sequence of both *BRAF* exon 15 and rs7801086. In all four patient samples, colonies with $BRAF^{V600E}$ as well as wild-type *BRAF* were accompanied by different SNP alleles, some harboring the G allele and others harboring the T allele. In sample number 14, one colony (*) showed a tandem $BRAF^{V600E/K601E}$ (T1799→A and A1802→G) mutation.

(T1799→A) mutation and the G allele of SNP rs7801086. Colonies that contained wild-type *BRAF* also harbored both G and T alleles. We used a high fidelity *Taq* polymerase in the PCR and did not find any base substitutions other than those encoding T1799A in exon 15 of the *BRAF* gene, except in one bacterial subclone from sample number 14 that carried a $BRAF^{V600E/K601E}$ (T1799→A and A1802→G) tandem mutation. These results indicate that even the same type of $BRAF^{V600E}$ mutation could originate from different cells in the same nevus and that multiple *BRAF* mutations were possible among the cells within a given nevus. Collectively, our data strongly suggest marked polyclonality of *BRAF* mutations in acquired melanocytic nevi.

This result suggests that acquired melanocytic nevi may be polyclonal lesions, of multicellular origin, that result from random proliferation of cells containing wild-type *BRAF* as well as cells containing mutant *BRAF*. The polymorphic X-linked human androgen receptor gene has been used previously to show that acquired melanocytic nevi are of clonal origin (12). However, a recent study questioned the validity of the human androgen receptor gene as a marker of tumor clonality because the clonal patch is relatively large in humans, often greater than 4 mm in diameter in the aorta, and even larger in the colon and breast, and because polyclonality can only be demonstrated at the borders of X-inactivation patches (13).

The reason why melanocytes in acquired melanocytic nevi are so susceptible to mutation is unknown. One possibility is that

genetically aberrant clones of melanocytes might already exist in the lesional skin of acquired melanocytic nevi, which would expand and acquire multiple mutations from stimuli such as UV radiation. Alternatively, the *BRAF* mutation might be a second hit after the clonal proliferation of nevus cells, which is initiated by either an as yet unknown mutation or other mechanisms. Cell proliferation itself may render melanocytes prone to mutation by the leakage of genotoxic species, such as reactive oxygen species (14).

It should be noted that most of the melanocytic nevi we examined were Unna's nevi and Miescher's nevi. We did not examine Clark's nevi, which are most commonly seen in adult Caucasians and are sometimes seen in association with melanoma (15). Nevertheless, polyclonality of *BRAF* mutations in the lesions of acquired melanocytic nevi suggests an alternative to the view that *BRAF* mutation is an initial event in melanocytic neoplasia (5).

References

1. Davies H, Bignell GR, Cox C, et al. Mutations of the BRAF gene in human cancer. *Nature.* 2002;417(6892):949–954.
2. Pollock PM, Harper UL, Hansen KS, et al. High frequency of BRAF mutations in nevi. *Nat Genet.* 2003;33(1):19–20.
3. Michaloglou C, Vredeveld LC, Soengas MS, et al. BRAFE600-associated senescence-like cell cycle arrest of human naevi. *Nature.* 2005;436(7051):720–724.
4. Gray-Schopfer VC, Cheong SC, Chong H, et al. Cellular senescence in naevi and immortalisation in melanoma: a role for p16? *Br J Cancer.* 2006;95(4):496–505.
5. Michaloglou C, Vredeveld LC, Mooi WJ, Peeper DS. BRAF(E600) in benign and malignant human tumours. *Oncogene.* 2008;27(7): 877–895.
6. Ichii-Nakato N, Takata M, Takayanagi S, et al. High frequency of BRAFV600E mutation in acquired nevi and small congenital nevi, but low frequency of mutation in medium-sized congenital nevi. *J Invest Dermatol.* 2006; 126(9):2111–2118.
7. Goto Y, Arigami T, Kitago M, et al. Activation of Toll-like receptors 2, 3, and 4 on human melanoma cells induces inflammatory factors. *Mol Cancer Ther.* 2008;7(11):3642–3653.
8. Campoli MR, Chang CC, Kageshita T, Wang X, McCarthy JB, Ferrone S. Human high molecular weight-melanoma-associated antigen (HMW-MAA): a melanoma cell surface chondroitin sulfate proteoglycan (MSCP) with biological and clinical significance. *Crit Rev Immunol.* 2004;24(4):267–296.
9. Wan PT, Garnett MJ, Roe SM, et al. Mechanism of activation of the RAF-ERK signaling pathway by oncogenic mutations of B-RAF. *Cell.* 2004;116(6):855–867.
10. Piyamongkol W, Bermudez MG, Harper JC, Wells D. Detailed investigation of factors influencing amplification efficiency and allele drop-out in single cell PCR: implications for preimplantation genetic diagnosis. *Mol Hum Reprod.* 2003;9(7):411–420.
11. Sumimoto H, Imabayashi F, Iwata T, Kawakami Y. The BRAF-MAPK signaling pathway is essential for cancer-immune evasion in human melanoma cells. *J Exp Med.* 2006;203(7):1651–1656.
12. Robinson WA, Lemon M, Elefanty A, Harrison-Smith M, Markham N, Norris D. Human acquired naevi are clonal. *Melanoma Res.* 1998;8(6):499–503.
13. Novelli M, Cossu A, Oukrif D, et al. X-inactivation patch size in human female tissue confounds the assessment of tumor clonality. *Proc Natl Acad Sci USA.* 2003;100(6): 3311–3314.
14. Miranda M, Amicarelli F, Poma A, et al. Cytogenotoxic species leakage within human melanoma melanosomes. Molecular-morphological correlations. *Biochem Mol Biol Int.* 1994; 32(5):913–922.
15. Ackerman AB, Magana-Garcia M. Naming acquired melanocytic nevi. Unna's, Miescher's, Spitz's, Clark's. *Am J Dermatopathol.* 1990; 12(2):193–209.

Funding

Grant-in-Aid for Cancer Research from the Ministry of Health, Labor, and Welfare of Japan (15–10 to T.S.) and by Public Health Service grant awarded by the National Cancer Institute (R01 CA105500 to S.F.). J.L. is a PhD student supported by the Ministry of Education, Culture, Sports, Science and Technology of Japan.

Notes

The study sponsor(s) had no role in the design of the study; the collection, analysis, or interpretation of the data; the writing of the manuscript; or the decision to submit the manuscript for publication.

Manuscript received November 4, 2008; revised July 21, 2009; accepted August 10, 2009.

Multiple Antigen-targeted Immunotherapy With α-Galactosylceramide–loaded and Genetically Engineered Dendritic Cells Derived From Embryonic Stem Cells

Satoshi Fukushima,† ‡ Shinya Hirata,* Yutaka Motomura,* Daiki Fukuma,* Yusuke Matsunaga,*‡ Yoshiaki Ikuta,* Tokunori Ikeda,*‡ Toshiro Kageshita,† Hironobu Ihn,† Yasuharu Nishimura,* and Satoru Senju*‡*

Summary: Numerous tumor-associated antigens (TAA) have been identified and their use in immunotherapy is considered to be promising. For TAA-based immunotherapy to be broadly applied as standard anticancer medicine, methods for active immunization should be improved. In the present study, we demonstrated the efficacy of multiple TAA-targeted dendritic cell (DC) vaccines and also the additive effects of loading α-galactosylceramide to DC using mouse melanoma models. On the basis of previously established methods to generate DC from mouse embryonic stem cells (ES-DC), 4 kinds of genetically modified ES-DC, which expressed the melanoma-associated antigens, glypican-3, secreted protein acidic and rich in cysteine, tyrosinase-related protein-2, or gp100 were generated. Anticancer effects elicited by immunization with the ES-DC were assessed in preventive and also therapeutic settings in the models of peritoneal dissemination and spontaneous metastasis to lymph node and lung. The in vivo transfer of a mixture of 3 kinds of TAA-expressing ES-DC protected the recipient mice from melanoma cells more effectively than the transfer of ES-DC expressing single TAA, thus demonstrating the advantage of multiple as compared with single TAA-targeted immunotherapy. Loading ES-DC with α-galactosylceramide further enhanced the anticancer effects, suggesting that excellent synergic effects of TAA-specific cytotoxic T lymphocytes and natural killer T cells against metastatic melanoma can be achieved by using genetically modified ES-DC. With the aid of advancing technologies related to pluripotent stem cells, induced pluripotent stem cells, and ES cells, clinical application of DC highly potent in eliciting anticancer immunity will be realized in the near future.

Key Words: cancer immunotherapy, dendritic cells, embryonic stem cells, tumor-associated antigen, α-GalCer

(*J Immunother* 2009;00:000–000)

Received for publication August 9, 2008; accepted November 2, 2008.

From the Departments of *Immunogenetics; †Dermatology and Plastic and Reconstructive Surgery, Graduate School of Medical Sciences, Kumamoto University, Kumamoto; and ‡Japan Science and Technology Agency, CREST, Tokyo, Japan.

Financial Disclosure: All of authors have declared there are no financial conflicts of interest related to this work.

Supported in part by Grants-in-Aid 18014023, 19591172, and 19059012 from the Ministry of Education, Science, Technology, Sports, and Culture (MEXT), Japan; the Program of Founding Research Centers for Emerging and Reemerging Infectious Diseases launched as a project commissioned by MEXT, Japan; Research Grant for Intractable Diseases from Ministry of Health and Welfare, Japan and Uehara Memorial Foundation; and Takeda Science Foundation.

Reprints: Satoru Senju, Department of Immunogenetics, Graduate School of Medical Sciences, Kumamoto University, 1-1-1 Honjo, Kumamoto 860-8556, Japan (e-mail: senjusat@gpo.kumamoto-u.ac.jp).

A number of preclinical studies have demonstrated the efficacy of cancer vaccines using mouse models. However, cancer vaccine trials in humans have yet to demonstrate a sufficient clinical response,[1,2] and at present tumor-associated antigens (TAA)-specific cancer immunotherapies are not regarded as the standard medical technology, except for several antibody therapies. Therefore, there is discrepancy between the promising results obtained in mouse studies and those of clinical trials. Although the reasons for this discrepancy vary, one is the improper selection of mouse models.[3] Most mouse studies use models where the tumor cells are inoculated subcutaneously or intravenously. These are convenient to observe the efficacy of immunotherapy. However, to evaluate the efficacy in clinical medicine, experimental systems should be used that reflect the clinical situations where immunotherapy is actually needed, such as cancers accompanying with multiple metastases or with peritoneally disseminated lesions. The present study evaluated the capacity of genetically engineered dendritic cells (DC) to inhibit peritoneal dissemination and spontaneous metastasis of mouse melanoma to lymph node and lungs.

Another issue to be considered is whether it is appropriate to design clinical strategies that combine multiple agents to modulate the immune response.[2] Clinically manifested cancers are often associated with multiple mechanisms to evade immune attacks, such as antigen loss, active tolerance induction, deficiency in antigen presentation machineries,[4] etc., which are difficult to be addressed successfully with a single agent. To overcome this defense mechanism and to address the low frequency of cytotoxic T lymphocytes (CTL) that recognize single endogenous TAA, the efficacy of multiple TAA-targeted immunotherapies was examined in the present study. DC were generated expressing endogenous TAA, glypican-3 (GPC3), secreted protein acidic and rich in cysteine (SPARC), tyrosinase-related protein-2 (TRP2), and gp100. The oncofetal protein GPC3, glycosylphosphatidylinositol anchored membrane protein, is specifically overexpressed in human melanoma and hepatocellular carcinoma, and GPC3 can be a candidate target for cancer immunotherapy.[5–7] Clinical trials with GPC3 peptide against hepatocellular carcinoma are now ongoing. SPARC, also called osteonectin, is a matricellular glycoprotein that modulates cellular interactions with the extracellular matrix during tissue remodeling.[8] SPARC or its combination with GPC3 is a useful tumor maker for melanoma.[9,10]

The manipulation of DC, specialized antigen-presenting cells, is a promising strategy to improve the efficacy of cancer immunotherapy.[11,12] Genetic modification to express antigenic proteins has several advantages in comparison with using a peptide, protein, or tumor cell lysate as a means for loading TAA to DC.[13] The expression of TAA by DC circumvents the need for identifying specific CTL epitopes within the protein, and the antigens are continuously supplied for presentation as opposed to a single pulse of peptides or tumor cell lysates.[14] Furthermore, in vivo transfer of DC transfected with TAA gene are able to prime CTL reactive to multiple TAA-derived epitopes.[15] Others and we have established to generate DC in vitro from mouse embryonic stem (ES) cells (ES-DC).[16,17] ES-DC have the capacity to stimulate T cells, present antigen, and migrate to lymphoid tissues upon in vivo administration, and their capacity is comparable with that of bone marrow-derived DC.[15,17–19] The genetic modification of ES-DC can be carried out without the use of viral vectors by introducing exogenous genes into undifferentiated ES cells by electroporation and the subsequent induction of their differentiation into ES-DC. In a previous study, ES-DC expressing GPC3 showed protective immunity against mouse melanoma, however, the therapeutic effects were insufficient.[15] To counter the cancers with deficiencies in antigen presentation machineries, it is necessary to induce the innate immunity. Alpha-galactosylceramide (α-GalCer) presented by DC efficiently stimulates natural killer T (NKT) cells.[20] Therefore, it is presumed that the in vivo transfer of DC simultaneously loaded with TAA and α-GalCer may stimulate both tumor-reactive T cells and NKT cells, resulting in a potent anticancer immunity. The present study investigated the anticancer effects of multiple TAA-targeted immunotherapies with α-GalCer–loaded and genetically engineered ES-DC against mouse melanoma.

MATERIALS AND METHODS

Mice

C57BL/6 mice were obtained from Japan SLC Inc. (Hamamatsu, Japan) and maintained under specific pathogen-free conditions. All studies were performed with C57BL/6 mice syngeneic to the mouse ES cell line B6 at 6 to 8 weeks of age. The mouse experiments were approved by the Animal Research Committee of Kumamoto University.

Cell Lines

The ES cell line B6, derived from C57BL/6 blastocysts, was kindly provided by Drs H. Suemori and N. Nakatsuji (Kyoto University). The method for in vitro induction of differentiation of ES cells into DC was described previously,[17] and ES-DC prepared from a 7-day culture in the presence of granulocyte-macrophage colony-stimulating factor were used for all assays. The C57BL/6-derived tumor cell lines, F10 and BL6 sublines of B16 melanoma, a fibrosarcoma cell line MCA205 (MCA), and a thymoma cell line EL-4 were provided by the Cell Resource Center for Biomedical Research Institute of Development, Aging, and Cancer, Tohoku University (Sendai, Japan). The cells were cultured in Roswell Park Memorial Institute-1640 supplemented with 10% horse serum. To produce GPC3-expressing MCA (MCA-GPC3), MCA cells were transfected with pCAGGS-GPC3-internal ribosomal entry site (IRES)–puromycin-resistant (puro-R) by using Lipofectamine 2000 (Invitrogen, Carlsbad, CA), selected with puromycin, and then subjected to cloning by limiting dilution as described previously.[15,21] To produce EL-4–expressing secreted protein acidic and rich in cysteine (EL-4–SPARC), EL-4 cells were transfected with pCAGGS-SPARC-IRES–puro-R same as above. Plasmid DNA encoding firefly luciferase was kindly provided by Dr M. Nishikawa (Kyoto University), and B16-BL6 cells were transfected with the construct as described above, then the single colonies of G418-resistant cells were picked up, and a clone was selected on the basis of the luciferase activity (B16-BL6/Luc).

Peptides and Cytokines

Known $CD8^+$ T-cell epitope peptides were purchased from AnyGen (Gwangju, Korea) and their amino acid sequences are as follows: mouse $TRP2_{180\text{-}188}$ (SVYDFFVWL, H-$2K^b$ restricted), mouse $gp100_{25\text{-}33}$ (EGSRNQDWL, H-$2D^b$ restricted), and human $gp100_{25\text{-}33}$ (KVPRNQDWL, H-$2D^b$ restricted). A control peptide derived from $OVA_{257\text{-}264}$ (SIINFEKL, H-$2K^b$ restricted) was synthesized by the automatic peptide synthesizer (PSSM8, SHIMADZU, Kyoto, Japan) and subsequently purified by high-performance liquid chromatography. Recombinant mouse granulocyte-macrophage colony-stimulating factor, recombinant human interleukin (IL)-2, recombinant murine interferon (IFN)-γ (PeproTechLondon, UK), and IL-4 (ProSpecTechnoGene, Rehovot, Israel) were purchased. Alpha-GalCer was kindly provided by Kirin Brewery Co (Tokyo, Japan).

Generation of ES-DC expressing GPC3, SPARC, TRP2, or Human gp100

cDNA fragments encoding for total mouse SPARC and TRP2 were obtained by reverse transcription polymerase chain reaction (RT-PCR) from B16-F10. Full-length mouse GPC3 and human gp100 (hgp100) cDNA clones were purchased from Invitrogen. cDNA fragments encoding the whole GPC3 protein and a fragment of hgp100 ($hgp100_{1\text{-}300}$) including the H-$2D^b$–restricted epitope ($hgp100_{25\text{-}33}$) were isolated from those clones. cDNA for GPC3, SPARC, TRP2, or hgp100 was transferred to a mammalian expression vector pCAGGS-IRES–puro-R, containing the CAG promoter and an IRES–puro-R gene cassette,[22,23] to generate an expression vector for GPC3, SPARC, TRP2 and hgp100, pCAGGS-GPC3-IRES–puro-R, pCAGGS-SPARC-FLAG-HA-IRES–puro-R, pCAGGS-TRP2-HA-IRES–puro-R, and pCAGGS-hgp100-HA-IRES–puro-R. All constructs contain HA-tag or FLAG-tag except for that of GPC3 (Fig. 1A). To generate transfectant ES cell clones, B6 ES cells were transfected with the expression vectors by electroporation and selected with puromycin as described previously.[17] Transfectant ES cell clones were subjected to a differentiation culture to generate ES-DC as described previously.[24,25] ES-DC differentiated from GPC3-transfectant, SPARC-transfectant, TRP2-transfectant, or hgp100-transfectant ES cells were designated as ES-DC–GPC3, ES-DC–SPARC, ES-DC–TRP2, or ES-DC–hgp100, respectively. Recombinant mouse IL-4 was given to ES-DC at 20 hours before in vivo transfer.

RT-PCR

Total cellular RNA was extracted by using the RNeasy Mini Kit (QIAGEN, Maryland, MD) and RT-PCR was carried out as previously described.[24] Briefly, total RNA was converted into cDNA and PCR was carried out for 30 cycles for the quantification of *GPC3*, *SPARC*, *TRP2*, *hgp100*, and glyceraldehyde-3-phosphate dehydrogenase

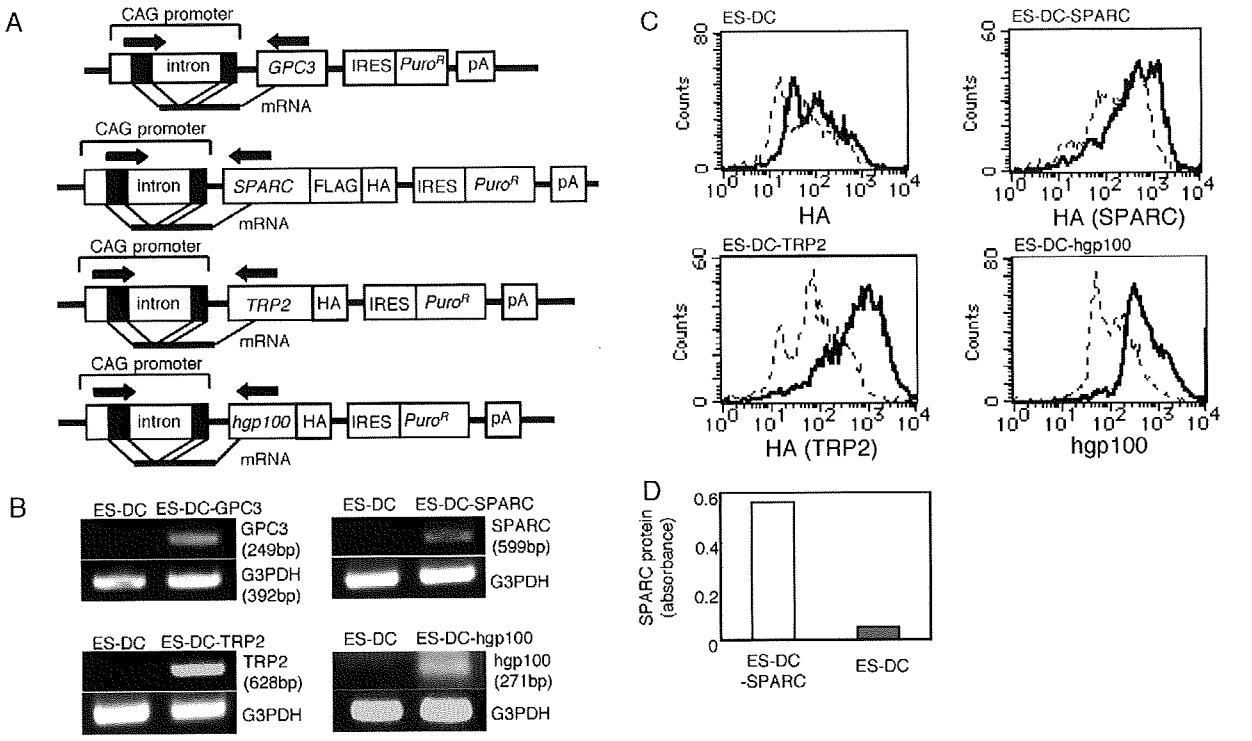

FIGURE 1. The generation of ES-DC expressing melanoma-associated antigens. A, Structure of vectors: pCAGGS-GPC3-IRES–puro-R, pCAGGS-SPARC-FLAG-HA-IRES–puro-R, pCAGGS-TRP2-HA-IRES–puro-R, and pCAGGS-hgp100-HA-IRES–puro-R. To obtain the vectors, each cDNA fragment encoding for a full-length of mouse *GPC3*, *SPARC*, *TRP2*, or $hgp100_{1\text{-}300}$ was inserted into a mammalian expression vector, pCAGGS-IRES–puro-R containing the CAG promoter, and an IRES–puro-R gene cassette. All constructs contain HA-tag or FLAG-tag except for that of GPC3. B, Expression of *GPC3*, *SPARC*, *TRP2*, and *hgp100* mRNA detected by RT-PCR in transfectant ES-DC. Primer sets (arrows in A) were designed to span the intron (917 bp) in the CAG promoter sequence to distinguish the PCR products of mRNA origin from the genome-integrated vector DNA origin. C, The expression of the transfected protein in ES-DC. Transfectant ES-DC were analyzed by flow cytometric analysis using intracellular staining. The staining patterns of specific antibodies (thick line) and negative control (dotted line) are shown. Anti-HA antibodies were used for staining of ES-DC, ES-DC–SPARC, and ES-DC–TRP2 and anti-hgp100 antibodies were used for staining of ES-DC–hgp100. D, SPARC protein secreted from ES-DC–SPARC or ES-DC (negative control) was measured by enzyme-linked immunosorbent assay. ES-DC indicates embryonic stem cell-derived dendritic cells; GPC3, glypican-3; hgp100, human gp100; IRES, internal ribosomal entry site; puro-R, puromycin-resistant; RT-PCR, reverse transcription polymerase chain reaction; SPARC, secreted protein acidic and rich in cysteine; TRP2, tyrosinase-related protein-2.

mRNA. The primer sequences for detection of the transgene in ES-DC and endogenous genes expressed in tumor cells are shown in Table 1. The sense strand primer used for detection of transgene-derived mRNA corresponded to the 5′ untranslated region included in the vector DNA. PCR products were visualized by ethidium bromide staining after separation by electrophoresis in a 1.5% agarose gel.

Flow Cytometric Analysis and Enzyme-linked Immunosorbent Assay

The staining of cells and the analysis on a flow cytometer (FACScan, BD Bioscience, San Jose, CA) were performed as previously described.[24,26] The antibodies and reagents used for staining were: fluorescein isothiocyanate (FITC)-conjugated anti-HA [clone 3F10, rat immunoglobulin (Ig) G1, Fab fragments, Roche, Indianapolis, IN], rabbit anti-gp100 (AnaSpec, San Jose, CA), FITC-conjugated goat antirabbit IgG (clone ALI4408, Biosource, Camarillo, CA), antimouse CD16/CD32 (clone 2.4G2, rat IgG2b BD Bioscience), recombinant soluble dimeric mouse CD1d:Ig (BD Bioscience), phycoerythrin-conjugated antimouse IgG1 (clone A85-1, rat IgG1, BD Bioscience), mouse IgG1 isotype control (clone A111-3, mouse IgG1, BD Bioscience), FITC-conjugated antimouse T-cell receptor (TCR) β (clone H57-597, hamster IgG, BD Bioscience), and IntraPrep permeabilization reagent (Beckman Coulter, Fullerton, CA). Enzyme-linked immunosorbent assay (ELISA) was carried out as described previously.[5,10] The concentrations of HA and FLAG-tagged SPARC proteins in the culture supernatants of ES-DC were measured by ELISA in triplicate wells using anti-FLAG (clone M2; mouse IgG, SIGMA, St Louis, MO) and anti–HA-peroxidase (clone 3F10; rat IgG1, Roche).

Induction of TAA-specific CTL and Cytotoxicity Assay

The mice were immunized intraperitoneally (IP) with each ES-DC twice with a 7-day interval. Seven days after the second immunization, spleen cells were isolated from the mice and cultured (2.5×10^6/well) with ES-DC–GPC3, ES-DC–SPARC, ES-DC–TRP2 (7×10^4/well), or 0.1 μM hgp100 peptide in 24-well culture plates in Roswell Park Memorial Institute-1640 supplemented with 10% horse serum, recombinant human IL-2, and 2-mercaptoethanol. After culturing for 5 days, the cells were recovered and their cytotoxic activity was analyzed by 4-hour ^{51}Cr release

TABLE 1. Sequences of PCR Primers

	Sense	Antisense
PCR primers used for detection of transgenes expressed in ES-DC		
GPC3	5′-CTGACTGACCGCGTTACTCCCACA-3′*	5′-TAGCAGCATCGCCACCAGCAAGCA-3′
SPARC	5′-CTGACTGACCGCGTTACTCCCACA-3′*	5′-GGCAAAGAAGTGGCAGGAAG-3′
TRP2	5′-CTGACTGACCGCGTTACTCCCACA-3′*	5′-TGGGCAGTCAGGGAATGGAT-3′
hgp100	5′-CTGACTGACCGCGTTACTCCCACA-3′*	5′-GCACCTATCACAGCCAAATG-3′
G3PDH	5′-GGAAAGCTGTGGCGTGATG-3′	5′-CTGTTGCTGTAGCCGTATTC-3′
PCR primers used for detection of endogenous genes expressed in tumor cells		
SPARC	5′-ATGAGGGCCTGGATCTTCTTTCTC-3′	5′-TTAGATCACCAGATCCTTGTTGATGTCC-3′
TRP2	5′-CCTTTGCGTTGCCCTACT-3′	5′-CTAGGCTTCCTCCGTGTATCTCTT-3′
mgp100	5′-CCCGTGCTTGTGCTGAGTGCTCTG-3′	5′-ATGCTCGACCTGGACACTGGAC-3′

*The sense strand primer used for detection of transgene-derived mRNA corresponded to the 5′ untranslated region included in the vector DNA (Fig. 1A).
ES-DC indicates embryonic stem cell-derived dendritic cells; GPC3, glypican-3; G3PDH, glyceraldehyde-3-phosphate dehydrogenase; hgp100, human gp100; mgp100, mouse gp100; PCR, polymerase chain reaction; SPARC, secreted protein acidic and rich in cysteine; TRP2, tyrosinase-related protein-2.

assays using MCA, MCA-GPC3, B16-F10, EL-4, EL-4–SPARC, and peptide pulsed EL-4 as targets basically by the same method as described previously.[15] B16-F10 cells were pretreated with recombinant murine IFN-γ (1000 units/mL) before use as target cells as reported previously.[27]

Subcutaneous Tumor Model

The mice were immunized IP with ES-DC–SPARC or ES-DC–TRP2 twice on days −14 and −7, and B16-F10 cells were inoculated subcutaneously into the shaved back region on day 0. In some experiments, the mice were immunized with a mixture of ES-DC–GPC3, ES-DC–SPARC, and ES-DC–TRP2. The tumor sizes were determined biweekly in a blinded fashion and the survival rate was monitored. The tumor volume was calculated as follows: tumor volume (mm^3) = (length × width × height).

Measurement of Luciferase Activity

The cells or tissues were homogenized with 2 mL of lysis buffer (0.05% Triton X-100, 2 mM ethylenediaminetetraacetic acid, 0.1 M Tris, pH 7.8) and the homogenates were cleared by centrifugation at 10,000 × g for 5 minutes. Twenty-five microliter of the supernatant was mixed with 75 μL of dilution buffer (phosphate-buffered saline containing $CaCl_2$ 1.8 mM and $MgSO_4$ 0.82 mM) and 100 μL of luciferase assay buffer (Steadyliteplus, PerkinElmer, Norwalk, CT), and at 10 minutes after the mixing the light produced was measured for 1 second in a luminometer (Tristar LB941, Berthold Technologies, Bad Wildbad, Germany). The luciferase activity was converted to the number of tumor cells using a regression line ($y = 0.1134x^2 - 0.305x + 0.4213$; x = cell number, y = counts/s).

Experimental Peritoneal Dissemination

In the preventive experiments, the mice were immunized IP with ES-DC–SPARC, ES-DC–TRP2, ES-DC–hgp100, their mixture (ES-DC–STH), or nontransfectant ES-DC twice on days 0 and 7, and B16-BL6/Luc cells were inoculated IP into mice on day 14. On day 28, the mice were euthanized and the greater omentum and pancreas were excised together and then the total luciferase activities were measured. In 1 experiment, the luciferase activities of the liver, kidney, spleen, and peritoneum were also measured. In the therapeutic experiments, B16-BL6/Luc cells were inoculated IP into mice on day 0. On days 3 and 10, ES-DC were transferred IP into mice. On day 17, mice were euthanized and luciferase activities of the greater omentum and pancreas were measured. In some experiments, ES-DC were cultured in the presence of α-GalCer (100 ng/mL) or vehicle (0.00025% Polysorbate-20) for 20 hours, and washed twice before injection. In 1 experiment, free α-GalCer (1 μg/mouse/transfer) either with or without ES-DC was transferred.

Analysis of the Activation of NKT Cells

The activation of NKT cells in vitro was analyzed as previously described.[28] In the analysis of the activation of NKT cells in vivo, on day 0, ES-DC loaded with either α-GalCer or vehicle were transferred IP into mice. On days 1, 7, 17, or 27, the mice were euthanized and the cytotoxic activities of the whole spleen cells against Yac-1 cells were analyzed.

In Vivo Depletion Experiments

The mice were transferred IP twice with either α-GalCer or vehicle loaded ES-DC–STH on days 0 and 7, and B16-BL6/Luc cells were inoculated IP into mice on day 14. To deplete the specific types of cells, the mice were given a total of 4 IP transfers (days −2, 5, 12, and 19) of monoclonal antibodies (mAbs), ascites (0.1 mL/mouse/transfer) from hybridoma-bearing nude mice, or polyclonal rabbit antiasialo GM1 antibody (Wako, Tokyo, Japan; 20 μL/mouse/transfer). The mAbs used were rat antimouse CD4 mAb (clone GK1.5) and rat antimouse CD8 mAb (clone 2.43). Normal rat IgG (Sigma-Aldrich, St Louis, MO; 200 μg/mouse/transfer) was used as a control. The depletion of specific cell subsets by treatment with antibodies was confirmed by a flow cytometric analysis of spleen cells, which showed a > 90% specific depletion.

Spontaneous Metastasis Experiments

In the preventive experiments, α-GalCer–loaded ES-DC or ES-DC–STH were transferred IP into mice twice on days 0 and 7. On day 14, the footpad of mice was inoculated with B16-BL6/Luc cells. On day 35, mice were euthanized, the lungs were excised, and total luciferase activities were measured. In the therapeutic experiments, B16-BL6/Luc cells were inoculated into the footpad on day 0. On days 3 and 10, ES-DC were transferred IP into mice. On day 21, mice were euthanized and luciferase activities of the inguinal lymph nodes were measured.

Statistical Analysis

Two-tailed Student *t* test was used to determine the statistical significance of differences in the tumor growth

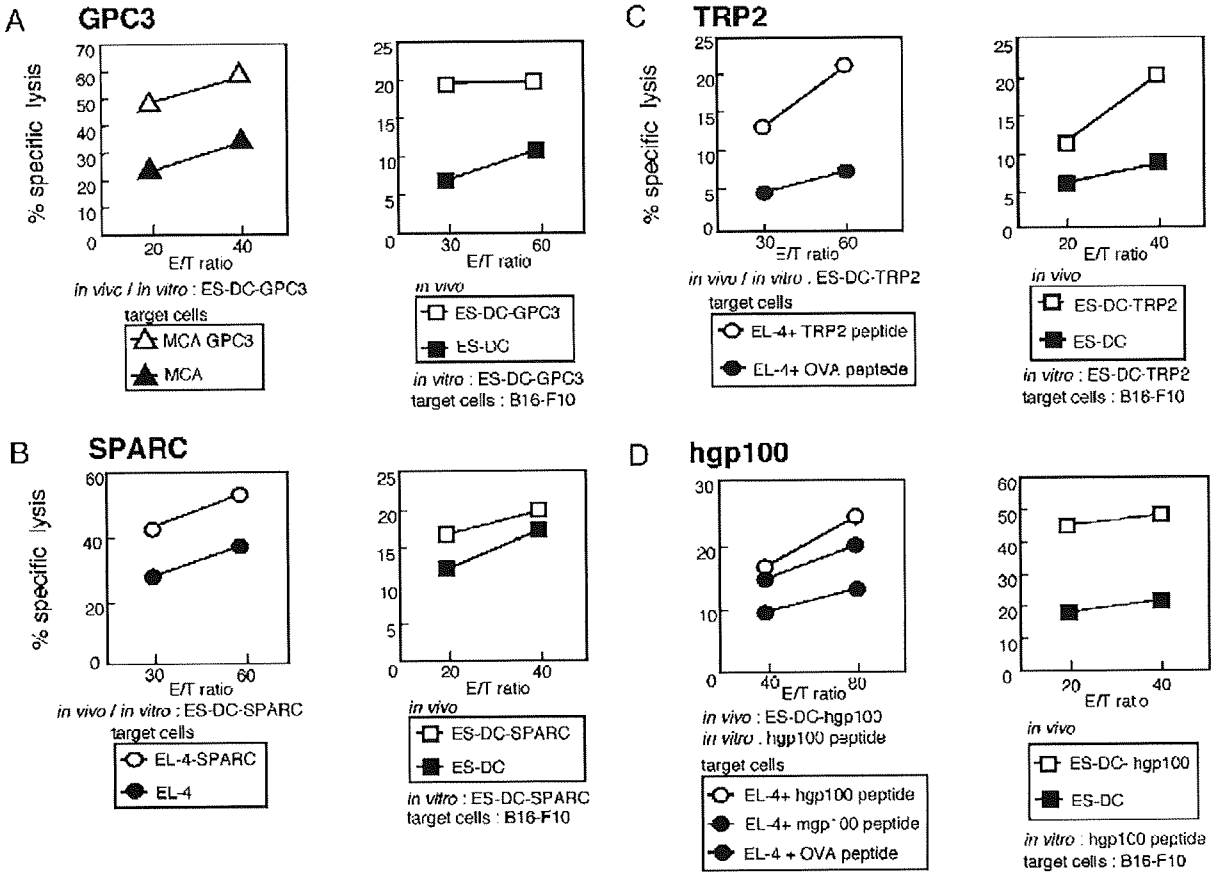

FIGURE 2. The priming of antigen-specific CTL in vivo with ES-DC expressing tumor-associated antigen. The mice were immunized intraperitoneally twice with each 1×10^5 ES-DC (as indicated in figure) on days 0 and 7. On day 14, spleen cells were isolated and cultured with 1×10^5 ES-DC–GPC3, ES-DC–SPARC, ES-DC–TRP2, or 0.1 μM human gp100 peptide per well in the presence of rhIL-2 (100 units/mL) for 5 days. Four-hour ^{51}Cr release assays were carried out using the obtained resultant cells to evaluate the capacity to kill MCA and MCA-GPC3 (A; left), EL-4 and EL-4–SPARC (B; left), EL-4 pulsed with the epitope peptide of TRP2 (C; left) and human or mouse gp100 (D; left), or B16-F10 (A–D; right). The results are expressed as percentage specific lysis from triplicate assays. The data are each representative of 2 independent experiments with similar results. CTL indicates cytotoxic T lymphocytes; ES-DC, embryonic stem cell-derived dendritic cells; GPC3, glypican-3; rhIL, recombinant human interleukin; SPARC, secreted protein acidic and rich in cysteine; TRP2, tyrosinase-related protein-2.

between the treatment groups. The Kaplan-Meier analysis with the Breslow-Gehan-Wilcoxon test was used to determine that of survival. The Mann-Whitney *U* test was used to examine the differences of luciferase activities. $P < 0.05$ was considered to be significant. Statistical analyses were performed by using the StatView 5.0 software package (Abacus Concepts, Calabasas, CA).

RESULTS

Generation of ES-DC expressing Melanoma Antigens

B6 ES cells were transfected with the *GPC3*, *SPARC*, *TRP2*, and *hgp100* expression vectors; pCAGGS-GPC3-IRES–puro-R, pCAGGS-SPARC-FLAG-HA-IRES–puro-R, pCAGGS-TRP2-HA-IRES–puro-R, pCAGGS-hgp100-HA-IRES–puro-R (Fig. 1A), and several transfectant clones were isolated. The transfectant ES cell clones were subjected to differentiation to ES-DC, and the transfectant clone expressing the highest level of each TAA was selected on the basis of the RT-PCR, fluorescence-activated cell sorting analysis, and ELISA (Fig. 1B–D).

Priming of TAA-specific CTL With Genetically Modified ES-DC

The capacity of ES-DC–GPC3, ES-DC–SPARC, ES-DC–TRP2, and ES-DC–hgp100 to prime each TAA-specific CTL was analyzed. Other investigators reported that immunization of mice with hgp100 elicited a mouse gp100-specific $CD8^+$ T-cell response more efficiently than that with mouse gp100.[29] Therefore, ES-DC expressing hgp100 were generated in the present study. The mice were immunized with ES-DC–GPC3, ES-DC–SPARC, ES-DC–TRP2, ES-DC–hgp100, or nontransfectant ES-DC, respectively, on days 0 and 7. On day 14, the spleen cells were isolated and cultured with ES-DC–GPC3, ES-DC–SPARC, ES-DC–TRP2, or hgp100 peptide for 5 days. Next, the cells were recovered and their TAA-specific killing activities were analyzed. For the analysis of GPC3-specific and SPARC-specific CTL, MCA-GPC3 and EL-4–SPARC were used as targets. For TRP2-specific and gp100-specific CTL, EL-4 cells pulsed with previously

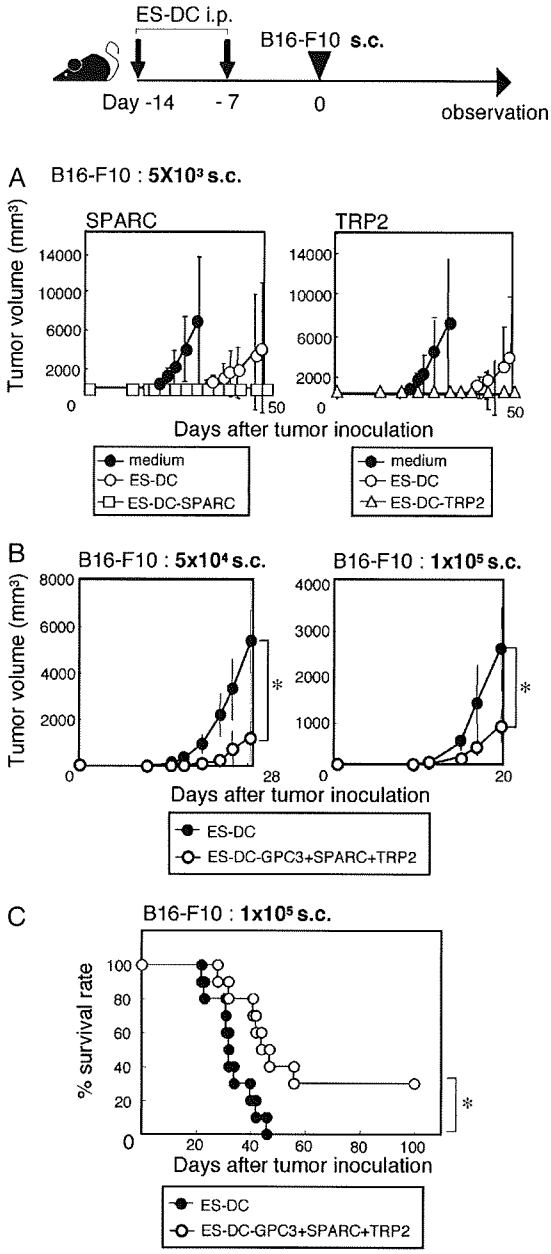

FIGURE 3. Protection against a subcutaneously inoculated tumor. A, About 1×10^5 ES-DC–SPARC or ES-DC–TRP2 were transferred IP into mice twice on days -14 and -7, and 5×10^3 B16-F10 cells were inoculated subcutaneously into the shaved back region on day 0. B, About 3×10^5 of nontransfectant ES-DC (control) or a mixture of ES-DC–GPC3, ES-DC–SPARC, and ES-DC–TRP2 that consisted of 1×10^5 of each ES-DC was transferred IP, and 5×10^4 or 1×10^5 B16-F10 cells were inoculated in the same schedule as above. The tumor sizes were determined biweekly in a blinded fashion and the survival rate was monitored (C). The tumor volume was calculated as follows: tumor volume (mm^3) = (length × width × height). The data are the mean ± SD (A–C, n = 5; D, n = 10; $*P<0.05$). The data are each representative of 2 independent experiments with similar results. ES-DC indicates embryonic stem cell-derived dendritic cells; GPC3, glypican-3; IP, intraperitoneal; SPARC, secreted protein acidic and rich in cysteine; TRP2, tyrosinase-related protein-2.

reported dominant epitopes of TRP2 and gp100 we used. As shown in Fig. 2A–D; left, the effector cells primed with ES-DC–GPC3, ES-DC–SPARC, ES-DC–TRP2, or ES-DC–hgp100 exhibited significantly higher killing activities against the target cells that specifically express each TAA. Furthermore, the effector cells activated with each TAA-expressing ES-DC in vivo showed significantly higher killing activities against the B16-F10 that naturally express each TAA (Fig. 2A–D; right). In contrast, spleen cells isolated from mice transferred with nontransfectant ES-DC and cocultured in vitro with each TAA exhibited a basal level killing activity. These results suggest that ES-DC–GPC3, ES-DC–SPARC, ES-DC–TRP2, and ES-DC–hgp100 have the capacity to prime TAA-specific CTL in vivo.

Protection Against Subcutaneously Inoculated Tumor

ES-DC–GPC3 can induce an antigen-specific protective effect against 5×10^3 subcutaneously inoculated B16-F10 cells naturally expressing GPC3.[15] However, the anticancer effect was insufficient when the mice were challenged with a larger number (1×10^4) of melanoma cells (unpublished observation). The present study examined whether ES-DC–SPARC or ES-DC–TRP2 could protect the recipient mice from a subcutaneous inoculation of 5×10^3 B16-F10 cells. Figure 3A shows that immunization with ES-DC–SPARC or ES-DC–TRP2 provided complete protection against 5×10^3 B16-F10 inoculations. We observed a certain antitumor effect of nontransfectant ES-DC (Fig. 3A). This phenomenon may be owing to the fact that even nontransfectant ES-DC produced cytokines with an antitumor effect, such as IL-12 and tumor necrosis factor-α. In addition, nontransfectant ES-DC may have presented tumor cell-derived TAA and activated specific CTL, as intrinsic natural DC did. However, the TAA-specific effect elicited by these ES-DC was not significant when the mice were inoculated with 5×10^4 B16-F10 cells (unpublished observation). Collectively, ES-DC expressing single TAA could protect the mice from subcutaneous challenge with a relatively small number of tumor cells, however, the effect was insufficient to protect the mice from a challenge with a larger number of tumor cells.

The simultaneous in vivo transfer of ES-DC–GPC3, ES-DC–SPARC, and ES-DC–TRP2 might protect the recipient mice from a challenge with a relatively large number of B16-F10 cells. Figure 3B demonstrates the transfer of a combination of these TAA-transfectant ES-DC to elicit a significant protection against inoculation with 5×10^4 and 1×10^5 B16-F10 cells, thus resulting in a significant prolongation of the survival time of the treated mice (Fig. 3C). Therefore, immunotherapy with multiple TAA is more effective than that with a single TAA.

Prevention of Peritoneal Dissemination of Melanoma by Preimmunization With Multiple TAA-targeted ES-DC

Experiments on preventing the growth of tumors inoculated subcutaneously are often performed and they are convenient models to observe the effects of cancer immunotherapy, but they do not accurately reflect clinical situations. In a preclinical study of cancer immunotherapy, it is important to examine in the metastatic models that are resistant to cancer immunotherapy. Therefore, the effects

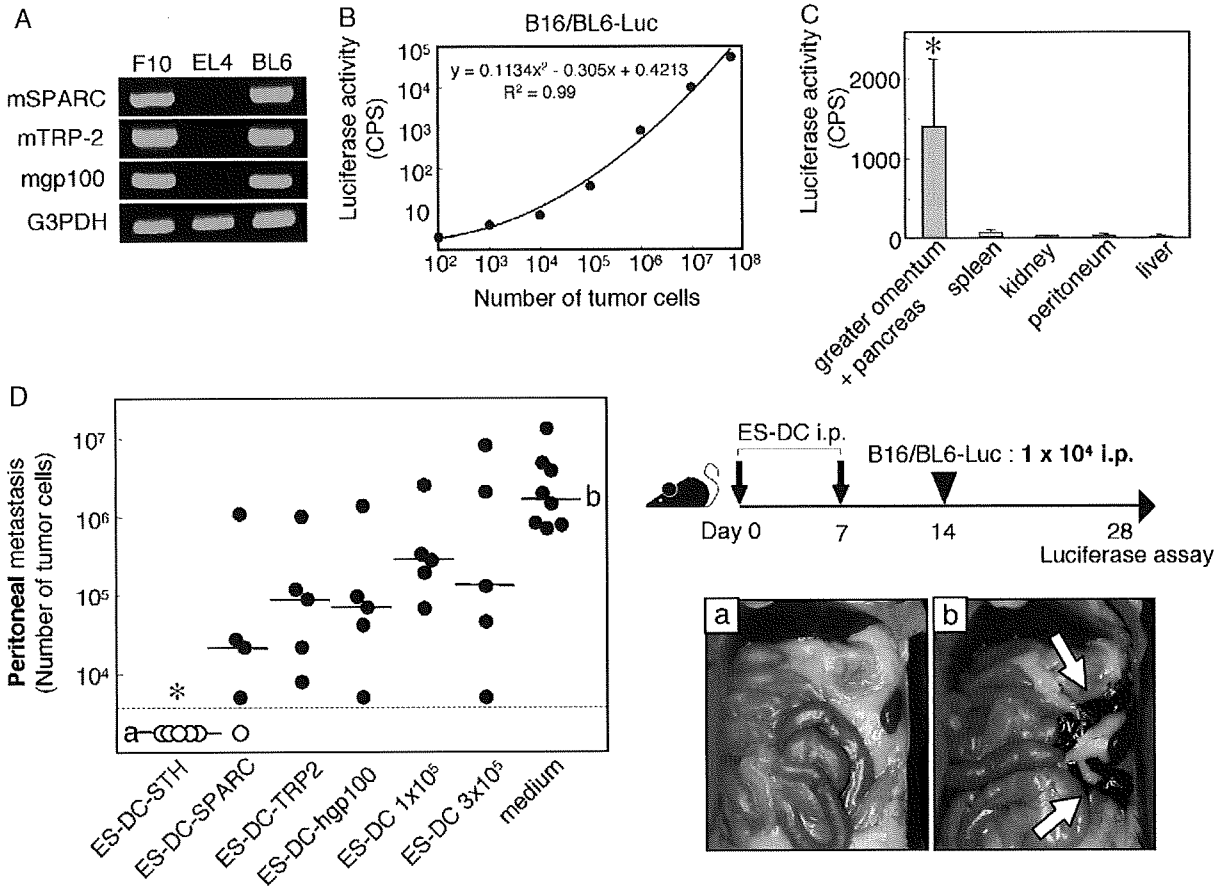

FIGURE 4. The prevention of peritoneal dissemination of melanoma by multiple tumor-associated antigen-targeted immunization with ES-DC. A, The expressions of SPARC, TRP2, and mouse gp100 mRNA in B16-BL6 were detected by RT-PCR. B, Luciferase activities in the homogenates of B16-BL6/Luc cells at the indicated numbers are shown. C, Luciferase activity of the homogenate of organs isolated on 17 days after IP inoculation of 1×10^4 B16-BL6/Luc cells. The data are shown as the counts per second (CPS). D, ES-DC–SPARC (1×10^5 cells), ES-DC–TRP2 (1×10^5 cells), ES-DC–hgp100 (1×10^5 cells), nontransfectant ES-DC (1×10^5 cells), nontransfectant ES-DC (3×10^5 cells), or a equal mixture of ES-DC–SPARC, ES-DC–TRP2, and ES-DC–hgp100 (ES-DC–STH; 3×10^5 cells in total) were inoculated IP into mice twice on days 0 and 7, and 1×10^4 B16-BL6/Luc cells were inoculated IP into mice on day 14. Mice were euthanized on day 28. The greater omentum and pancreas were excised together and the total luciferase activity was measured. The luciferase activity was converted to the number of tumor cells using a regression line shown in B. Typical examples of peritoneal dissemination of B16-BL6/Luc cells are shown in mice inoculated with (left; A) ES-DC–STH or (right; B) medium (C, n = 5; D, n = 5 to 8; $*P<0.05$). Dotted line indicates the detection limit. The data are each representative of 2 independent experiments with similar results. ES-DC indicates embryonic stem cell-derived dendritic cells; IP indicates intraperitoneal; RT-PCR, reverse transcription polymerase chain reaction; SPARC, secreted protein acidic and rich in cysteine; TRP2, tyrosinase-related protein-2.

of ES-DC were evaluated in the peritoneal dissemination model.[18,28] Previously, the survival rate was the only end point in the peritoneal dissemination model. To evaluate tumor metastasis, labeling of cells by introducing reporter gene is a promising technique because the metastatic cells can be quantified. A firefly luciferase gene was introduced into a mouse melanoma B16-BL6 cell line that is a highly metastatic subline of B16, as previously described[30] and established a transfectant clone B16-BL6/Luc. The expressions of *SPARC*, *TRP2*, and mouse *gp100* mRNA were detected by RT-PCR analysis in B16-BL6 (Fig. 4A) and *gpc3* mRNA was not detected (unpublished observation). The luciferase activities in the homogenates of B16-BL6/Luc cells indicated that the luciferase activity was correlated with the number of B16-BL6/Luc cells at least in the range from 7 to 60,000 counts/s (Fig. 4B). The luciferase activity of the homogenate of each organ was confirmed on day 17 after IP inoculation of 1×10^4 B16-BL6/Luc cells (Fig. 4C). As others have reported, the greater omentum and pancreas were the most common site of metastasis in the early stage of peritoneal dissemination.[31] Because the luciferase activities of the greater omentum and pancreas were significantly higher than other organs such as the spleen, liver, kidney, and peritoneum, the luciferase activities of greater omentum and pancreas were measured to evaluate the metastasis of abdominal organs in the subsequent experiments.

The preventive effects of ES-DC were evaluated in the peritoneal tumor dissemination model (Fig. 4D). Immunization with ES-DC–SPARC, ES-DC–TRP2, or ES-DC–hgp100 did not show a TAA-specific, antitumor effect to inhibit the dissemination when 1×10^4 B16-BL6/Luc cells were inoculated. However, simultaneous in vivo transfer of ES-DC–SPARC, ES-DC–TRP2, and ES-DC–hgp100 completely prevented the tumor dissemination.

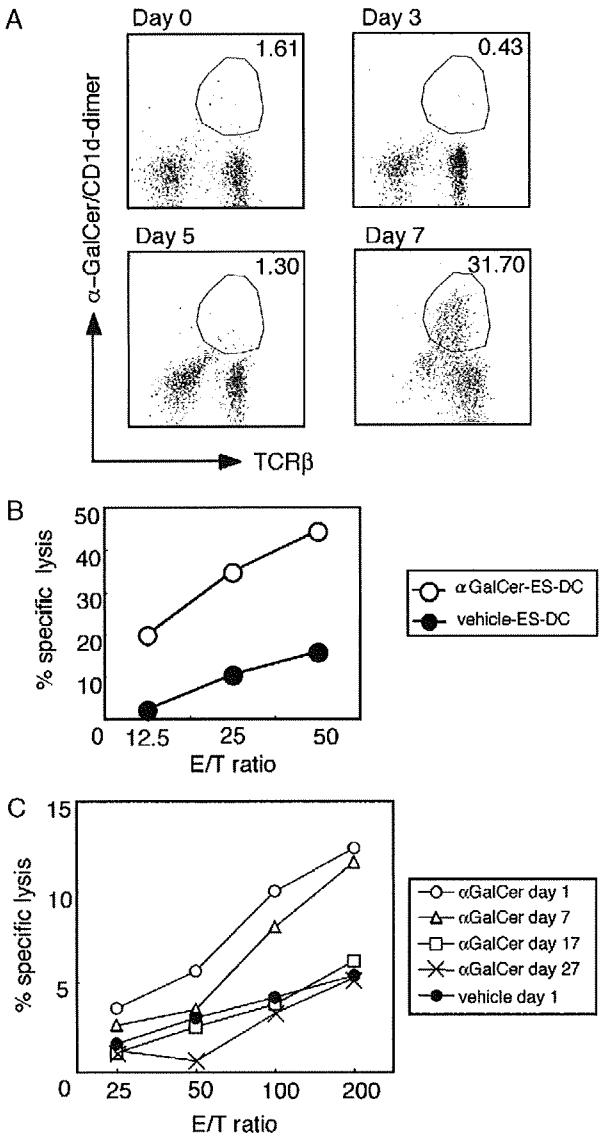

FIGURE 5. The activation of NKT cells by α-GalCer–loaded ES-DC. A, ES-DC were cultured in the presence of α-GalCer or vehicle alone for 20 hours, washed twice, and cocultured with splenic T cells of syngeneic mice (5×10^4 DC+2.5×10^6 T cells/well in 24-well culture plate). On day 0, 3, 5, or 7, the cells were analyzed by flow cytometric analysis. The percentage of NKT cells, defined as TCRβ$^+$ and α-GalCer/CD1d dimer reactive cells, is indicated. B, On day 5, the effecter cells recovered from the culture were analyzed for their cytotoxic activities by a 4-hour ^{51}Cr-release assay using Yac-1 cells as target cells (1×10^4 cells/well) at the indicated effecter:target ratio. C, In vivo activation of NKT cells by α-GalCer–loaded ES-DC. On day 0, ES-DC loaded with either α-GalCer or vehicle alone were transferred intraperitoneally into mice (1×10^6 cells/mouse). On day 1, 7, 17, or 27, the mice were euthanized and the cytotoxic activities of whole spleen cells against Yac-1 cells were analyzed, as described above. The results are expressed as percentage specific lysis from triplicate assays. ES-DC indicates embryonic stem cell-derived dendritic cells; NKT, natural killer T; TCR, T-cell receptor; α-GalCer, α-galactosylceramide.

Therefore, the potency of immunotherapy with multiple TAA was confirmed also in the peritoneal dissemination model.

Activation of NKT Cells by α-GalCer–loaded ES-DC

Others have reported that α-GalCer loaded on mature DC induced more prolonged IFN-γ production by NKT cells and better protection against B16 melanoma than free α-GalCer.[20] The capacity of ES-DC was first confirmed to activate NKT cells in vitro. As shown in Figure 5A, NKT cells detected by α-GalCer/CD1d dimer represented 1.61% of splenic T cells before stimulation with α-GalCer–loaded ES-DC (day 0). After stimulation, TCRβ$^+$ dimer$^+$ cells almost disappeared on day 3, probably reflecting activation-induced down-regulation of the surface TCR.[32,33] This population began to reappear on day 5 and was dramatically increased (31.7%) on day 7, consistent with previous reports that activated NKT cells remain quiescent for a while, but eventually proliferate. The cultured cells recovered on day 5 exhibited strong cytotoxic activities against Yac-1 cells (Fig. 5B). These results indicate that α-GalCer–loaded ES-DC induced significant activation and of NKT cells in vitro. Next, the duration of activation of NKT cells induced by ES-DC was analyzed in vivo. On day 0, ES-DC loaded with either α-GalCer or vehicle were injected IP into mice. On days 1, 7, 17, or 27, the mice were euthanized and the cytotoxic activity of whole spleen cells against Yac-1 cells was analyzed. Figure 5C showed the Yac-1 cell-killing activities of spleen cells reflecting activation of NKT cells. The killing activities sustained for 1 week, and after 2 weeks the effect decreased to the background level.

Potent Anticancer Effects of Multiple TAA-targeted ES-DC Loaded With α-GalCer

We evaluated the effects of multiple TAA-targeted and α-GalCer–loaded ES-DC in several metastatic models. As shown in Figure 6A, simultaneous in vivo transfer of vehicle-loaded ES-DC–SPARC, ES-DC–TRP2, and ES-DC–hgp100 did not show a significant inhibition of the dissemination of 5×10^4 B16-BL6/Luc cells, when 5 times more cells were injected IP in comparison with the experiments shown in Figure 4D. Although α-GalCer–loaded ES-DC without TAA induced a significant but a partial protection, a mixture of 3 kinds of TAA-transfectant ES-DC loaded with α-GalCer completely protected the mice from tumor dissemination. As shown in Figure 6B, α-GalCer–loaded ES-DC expressing TAA induced a significantly more potent protection than either 1 μg of free α-GalCer alone (the commonly used dose) or that injected simultaneously with ES-DC expressing TAA. These results clearly indicate the advantage of loading α-GalCer to DC to improve the anticancer effects. To analyze the effector cell populations induced by α-GalCer–loaded ES-DC with TAA, in vivo depletion of CD4$^+$T, CD8$^+$T, or natural killer (NK) cells with specific antibodies was performed as shown in Figure 6C. The preventive effects of the immunization with α-GalCer–loaded TAA-expressing DC (compared with vehicle-loaded TAA-expressing DC) were almost totally abrogated when CD4$^+$T cells, CD8$^+$T cells, or NK cells were depleted. These results suggest that all of 3 effector cell subsets were essential to achieve the protective effect.

Spontaneous pulmonary metastasis was induced by inoculation of B16-BL6/Luc cells into the footpad as previously described.[34] The mixture of α-GalCer–loaded ES-DC–SPARC, ES-DC–TRP2, and ES-DC–hgp100 or α-GalCer–loaded ES-DC without TAA were transferred

IP into mice twice on days 0 and 7. On day 14, 2×10^6 B16-BL6/Luc cells were inoculated into the footpad of mice. On day 35, the mice were euthanized, the lungs were excised, and luciferase activities were measured. As shown in Figure 7A, in vivo transfer of a mixture of 3 kinds of TAA-transfectant ES-DC loaded with α-GalCer induced significant protection compared with α-GalCer–loaded ES-DC without TAA also in the spontaneous pulmonary metastasis model. In this model, we have no evidence indicating that the loading of α-GalCer to TAA-expressing ES-DC provided any benefit in regard to inhibiting the local tumor growth in the primary lesion. This result may be owing to the tissue distribution of NKT cells. NKT cells are known to mainly localize in the liver, lung, spleen, bone marrow, and peritoneal cavity.

Finally, the effects of the in vivo transfer of a mixture of 3 kinds of TAA-transfectant ES-DC loaded with α-GalCer in the therapeutic setting on lymph node metastasis and peritoneal dissemination were evaluated. On day 0, 2×10^6 B16-BL6/Luc cells were inoculated into the footpad or 1×10^4 tumor cells were inoculated IP into mice. On days 3 and 10, ES-DC were transferred IP, and on day 21 or 17, respectively, the mice were euthanized and luciferase activities were measured. Multiple TAA-targeted ES-DC loaded with α-GalCer induced significant therapeutic effects compared with α-GalCer–loaded ES-DC without TAA in the model of spontaneous metastasis to inguinal lymph node (Fig. 7B). As shown in Figure 7C, although the in vivo transfer of α-GalCer–loaded ES-DC without TAA or vehicle-loaded ES-DC with TAA showed insufficient effects, a mixture of 3 kinds of TAA-transfectant ES-DC loaded with α-GalCer induced a significant therapeutic effect in the peritoneal dissemination model.

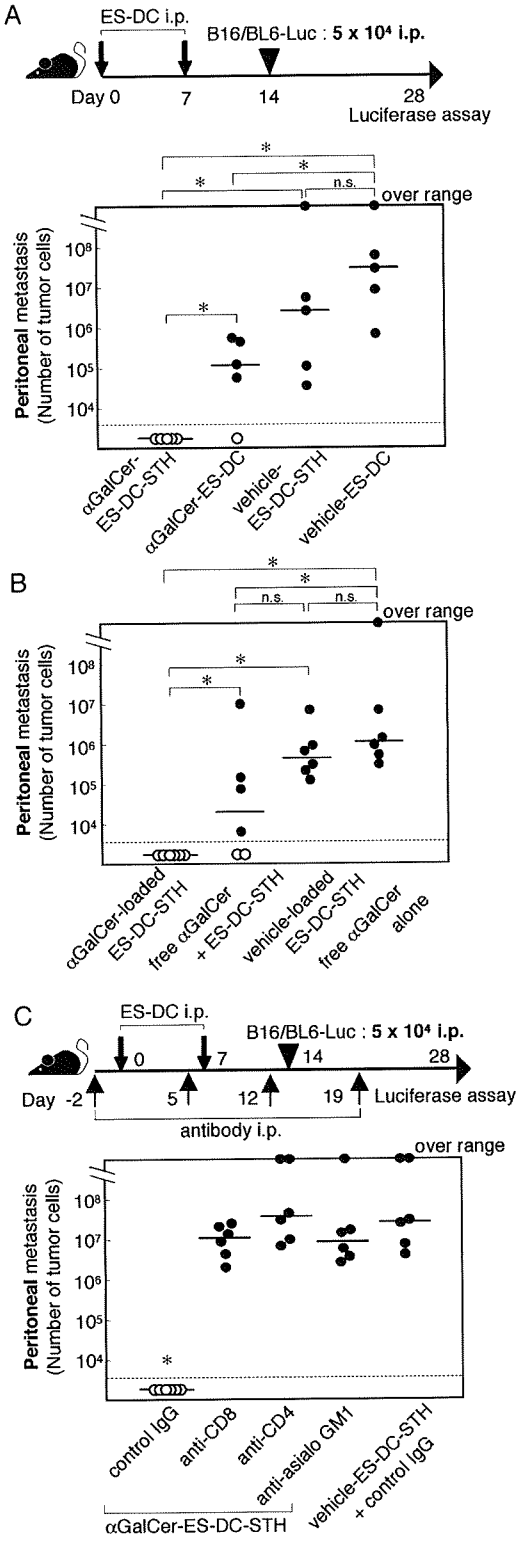

FIGURE 6. Preventive anticancer effects of multiple tumor-associated antigen-targeted vaccinations with α-GalCer–loaded ES-DC. A, The mixture of ES-DC–SPARC, ES-DC–TRP2, and ES-DC–hgp100 (3×10^5) loaded with either α-GalCer (αGalCer–ES-DC–STH) or vehicle (vehicle–ES-DC–STH) or nontransfectant ES-DC loaded with either α-GalCer (α-GalCer–ES-DC) or vehicle (vehicle–ES-DC) were transferred IP into mice twice on days 0 and 7, and 5×10^4 B16-BL6/Luc cells were inoculated IP into mice on day 14. On day 28, the mice were euthanized and the greater omentum and pancreas were excised together and the total luciferase activities were measured. B, 3×10^5 α-GalCer–loaded ES-DC–STH, free α-GalCer (1 μg/mouse/transfer) combined with ES-DC–STH, vehicle-loaded ES-DC–STH, and free α-GalCer alone (1 μg/mouse/transfer) were transferred IP into mice twice on days 0 and 7. About 5×10^4 B16-BL6/Luc cells were inoculated and luciferase activities were measured using the same protocol as A. C, $CD4^+$ T, $CD8^+$ T, or NK cells were depleted in vivo by the IP transfer of anti-CD4 mAb, anti-CD8 mAb, or polyclonal rabbit anti-asialo GM1 Ab. During this procedure, the mice were immunized with α-GalCer–loaded or vehicle-loaded ES-DC–STH and challenged IP with B16-BL6/Luc cells in the same protocol as A. Dotted line indicates the detection limit (A, n = 5; B and C, n = 6; *P<0.05). The data are each representative of 2 independent experiments with similar results. ES-DC indicates embryonic stem cell-derived dendritic cells; hgp100, human gp100; IP, intraperitoneal; mAb, monoclonal antibody; NK, natural killer; SPARC, secreted protein acidic and rich in cysteine; TRP2, tyrosinase-related protein-2; α-GalCer, α-galactosylceramide.

DISCUSSION

The anticancer effects of multiple TAA-targeted immunotherapies against mouse melanoma were evaluated by using α-GalCer–loaded and genetically engineered ES-DC. Four TAA that were naturally overexpressed in melanoma were selected, GPC3, SPARC, TRP2, and gp100. SPARC is expressed in various types of cancer tissues[35,36] and implicated in evasion of cancers from

immune attack.[37,38] The present study is the first to demonstrate that SPARC can be a target antigen for cancer immunotherapy. Figures 2B, 3A and 4D show that the effect of SPARC as the target antigen was comparable with the previously known melanoma-associated antigen, TRP2, or gp100.

CTL specific to each TAA were sensitized by the in vivo transfer of DC transfected with *GPC3*, *SPARC*, *TRP2*, or *hgp100* gene. However, the anticancer effects of ES-DC expressing single TAA in vivo were insufficient (Fig. 4D). These results are quite similar to the situation of recent T cell-targeted cancer immunotherapy. Using DC expressing multiple TAA for cancer immunotherapy makes sense and several studies have been reported.[39–41] However, there are very few reports that directly demonstrate the advantage of multiple as compared with single TAA-targeted immunotherapy.[42] As shown in Figures 3B, C and 4D, preimmunization with the mixture of 3 independent TAA transfectant ES-DC protected the mice more efficiently than the ES-DC expressing single TAA. The enhancement of antitumor immunity by the transfer of a mixture of 3 kinds of TAA-transfectant DC could be owing to an increase of number of CTL attacking tumor cells and a low frequency of immune escape.

In the past decade, α-GalCer has been attracting attention as a novel immunostimulatory reagent for cancer immunotherapy. CD1d is monomorphic and thus CD1d–α-GalCer–complex on DC can stimulate the NKT cells of any recipients. On the basis of the promising results of preclinical studies demonstrating the anticancer effects of α-GalCer–loaded DC,[20] several phase 1 clinical studies have been conducted. Although the activation and expansion of NKT cells by the administration of α-GalCer–loaded DC has been observed, the results seemed to be unsatisfactory from the viewpoint of the clinical effects.[43–46] The present study evaluated the effects of loading α-GalCer onto ES-DC–expressing endogenous TAA to induce anticancer immunity. Upon loading with α-GalCer, ES-DC had a capacity to activate NKT cells (Fig. 5). Figure 5C showed that the killing activity induced by the in vivo administration of α-GalCer–loaded ES-DC through the activation of NKT cells was sustained 1 week, and after 2 weeks the effect decreased to the background level. Despite this transient NKT cell activating capacity of α-GalCer–loaded ES-DC, anticancer effects induced by a mixture of 3 kinds of TAA-transfectant ES-DC loaded with α-GalCer showed a potent effect on inhibiting the growth of B16-BL6/Luc at 2 or 5 weeks after the administration as shown in Figures 6

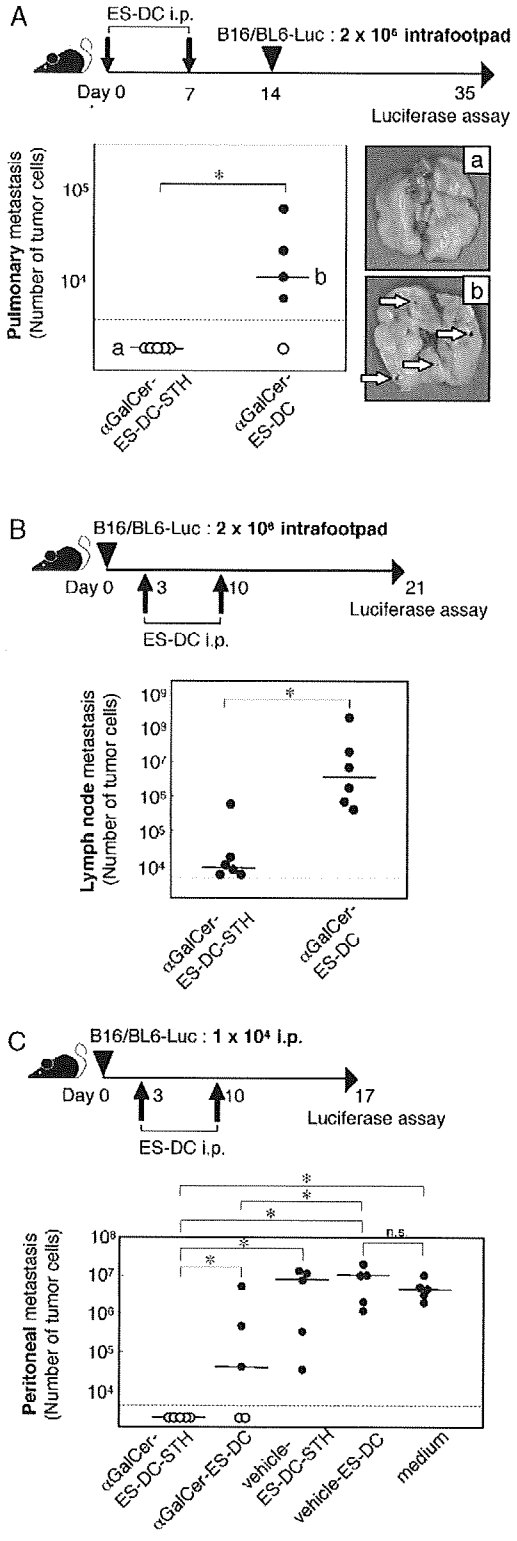

FIGURE 7. Potent anticancer effects of multiple tumor-associated antigen-targeted vaccinations with α-GalCer-loaded ES-DC. A, About 3×10^5 of α-GalCer–ES-DC–STH or α-GalCer–ES-DC were transferred IP into mice twice on days 0 and 7. On day 14, 2×10^6 B16-BL6/Luc cells were inoculated into the footpad of mice. On day 35, the mice were euthanized, the lungs were excised, and luciferase activities were measured. Typical examples of pulmonary metastasis of B16-BL6/Luc cells in mice are shown: above; A, α-GalCer–ES-DC–STH; below; B, α-GalCer–ES-DC. B, On day 0, 2×10^6 B16-BL6/Luc cells were inoculated into the footpad of mice. On days 3 and 10, each ES-DC was transferred IP. On day 21, the mice were euthanized and the luciferase activities of the inguinal lymph nodes were measured. C, On day 0, 1×10^4 B16-BL6/Luc cells were inoculated IP into mice. On days 3 and 10, each ES-DC was transferred IP. On day 17, the mice were euthanized and the luciferase activities of the greater omentum and pancreas were measured. Dotted line indicates the detection limit (A and C, n=5; B, n=6; *$P<0.05$). The data are each representative of 2 independent experiments with similar results. ES-DC indicates embryonic stem cell-derived dendritic cells; IP, intraperitoneal; α-GalCer, α-galactosylceramide.

and 7. In contrast, α-GalCer–loaded ES-DC without TAA showed an insufficient effect under the same conditions. This suggests that α-GalCer–loaded ES-DC have potent, antigen nonspecific effect in the early phase after administration, but sustained anticancer effect requires activation of TAA-specific CTL induced by ES-DC expressing TAA. Interestingly, the others reported that NKT cells activation induced by α-GalCer–loaded mature DC helped to boost adaptive immunity in vivo.[45] We performed an IFN-γ enzyme-linked immunosorbent spot assay to investigate whether the loading of α-GalCer to TAA-expressing DC would enhance the TAA-specific immunoresponse. However, no significant enhancement was observed when the mice were immunized with α-GalCer–loaded TAA-expressing DC in comparison with the vehicle-loaded TAA-expressing DC (unpublished observation). The preventive effects of the immunization with α-GalCer–loaded TAA-expressing DC (compared with vehicle-loaded TAA-expressing DC) were almost totally abrogated when the $CD4^+$ T cells, $CD8^+$ T cells, or NK cells were depleted (Fig. 6C). Collectively, we considered that the enhanced antitumor effects induced by α-GalCer–loaded TAA-expressing DC came from the cooperative work of $CD4^+$ T cells, $CD8^+$ T cells, and NK cells.

Anticancer immunotherapy with DC loaded with human leukocyte antigen (HLA)-binding peptides derived from TAA has been tested clinically in many institutions. In most cases, the DC are generated by culture of monocytes obtained from peripheral blood of the patients. To generate a sufficient number of DC for treatment, apheresis, a procedure that is sometimes invasive for patients with advanced stages of cancer, is necessary. In addition, the culture to generate DC should be carried out separately for each patient and treatment, and thus the procedure used at present may be too labor-intensive and expensive to be applied broadly in a practical setting. Alternately, the source of ES-DC, ES cells, has the capacity to propagate infinitely and multiple gene-transfectant ES-DC can be generated by the sequential transfection of ES cells with vectors bearing different selection markers.[18,24,25] Generation and genetic modification of ES-DC from human ES cells is achieved by the currently established method.[47] It may, therefore, be possible to generate multiple gene-transfectant human ES-DC expressing TAA plus immunostimulating molecules, which could thus more potently stimulate anticancer immunity than monocyte-derived DC do.

Considering the future clinical application of ES-DC, allogenicity (ie, differences in the genetic background) between patients to be treated and ES cells as a source for DC may cause problems. However, it is expected that human ES cells sharing some HLA alleles with the patients will be available for most cases. Mouse ES-DC administered into semiallogenic recipients, sharing 1 major histocompatibility complex (MHC) haplotype with the ES-DC, effectively primed antigen-specific CTL, thus suggesting that ES-DC can survive for a sufficient period to stimulate antigen-specific CTL restricted by the shared MHC class I.[48] However, in the same semiallogenic setting, the 5 times injection of nonantigen-loaded ES-DC significantly reduced the efficiency of priming of antigen-specific CTL induced by the subsequent injection of antigen-loaded ES-DC (unpublished observation). Therefore, repetitive stimulation with ES-DC expressing allogenic MHC may result in activation and expansion of allogenic MHC class I-reactive CTL, and in such recipients subsequently transferred ES-DC may be rapidly eliminated. Repeated immunization may be required in clinical applications to induce strong anticancer immunity. Therefore, the problem of the histoincompatibility between ES cell lines and recipients should be resolved. The methods for targeted gene modification of human ES cells and for targeted chromosome elimination of mouse ES cells have been developed. To overcome the problem of histoincompatibility, genetic modification to inhibit expression of endogenous HLA class I in ES-DC may be effective. A disruption of the genes for the molecules necessary for the cell surface expression of HLA class I molecules, such as transporter associated with antigen processing or β2-microglobulin (β2M), is presumably feasible. Along this line, we recently reported that the efficient activation of antigen-specific CTL was induced by TAP1 or β2M disrupted and recipient-matched MHC class I introduced mouse ES-DC.[19] We are now preparing to introduce expression vector encoding for β2M-linked form of recipient-matched HLA class I heavy chain into TAP1-deficient or β2M-deficient human ES cells.

Previous studies on ES-DC were performed by using well-established TT2 ES cells.[15,18,28] The present study confirmed that ES-DC could be generated from B6 ES cells with the same method previously established by using TT2 ES cells.[17] ES-DC generated from B6 ES cells were comparable with TT2 ES cells in differentiation, proliferation, surface phenotype, and antigen presentation. In addition, ES-DC could be generated from other ES cell lines (unpublished observation), thus suggesting that the method to generate ES-DC can be applied to various types of mouse ES cells.

Other studies have reported the generation of induced pluripotent stem (iPS) cells from adult human dermal fibroblasts with the defined 4 factors: Oct3/4, Sox2, Klf4, and c-Myc.[49] Human iPS cells are similar to human ES cells in morphology, proliferation, surface antigens, gene expression, epigenetic status of pluripotent cell-specific genes, and telomerase activity. DC can be generated from mouse iPS cells (unpublished observation) and testing is underway to determine whether DC could be generated from human iPS cells. Tailor-made medicine may, therefore, someday be possible if "iPS-DC" can be generated in the future.

ACKNOWLEDGMENTS

The authors thank Drs H. Suemori and N. Nakatsuji for B6, Dr M. Nishikawa for pCMV-Luc, and Kirin Brewery for α-GalCer.

REFERENCES

1. Rosenberg SA, Yang JC, Restifo NP. Cancer immunotherapy: moving beyond current vaccines. *Nat Med.* 2004;10:909–915.
2. Finke LH, Wentworth K, Blumenstein B, et al. Lessons from randomized phase III studies with active cancer immunotherapies—outcomes from the 2006 meeting of the Cancer Vaccine Consortium (CVC). *Vaccine.* 2007;25(suppl 2):B97–B109.
3. Ostrand-Rosenberg S. Animal models of tumor immunity, immunotherapy and cancer vaccines. *Curr Opin Immunol.* 2004;16:143–150.
4. Kageshita T, Ishihara T, Campoli M, et al. Selective monomorphic and polymorphic HLA class I antigenic determinant loss in surgically removed melanoma lesions. *Tissue Antigens.* 2005;65:419–428.
5. Nakatsura T, Yoshitake Y, Senju S, et al. Glypican-3, overexpressed specifically in human hepatocellular carcinoma,